

General Bayesian L^2 calibration of mathematical models

Antony M. Overstall

School of Mathematical Sciences, University of Southampton,
Southampton SO17 1BJ, U.K., A.M.Overstall@soton.ac.uk
and

James M. McGree

School of Mathematical Sciences, Queensland University of Technology,
Brisbane 4001, Australia, james.mcgree@qut.edu.au

December 23, 2024

Abstract

A general Bayesian method for L^2 calibration of a mathematical model is presented. General Bayesian inference starts with the specification of a loss function. Then, the log-likelihood in Bayes' theorem is replaced by the negative loss. While the minimiser of the loss function is unchanged by, for example, multiplying the loss by a constant, the same is not true of the resulting general posterior distribution. To address this problem in the context of L^2 calibration of mathematical models, different automatic scalings of the general Bayesian posterior are proposed. These are based on equating asymptotic properties of the general Bayesian posterior and the minimiser of the L^2 loss. The approach is validated and compared to traditional Bayesian calibration on a range of synthetic and real applications.

Keywords: loss functions, composite likelihood, curvature scaling, magnitude scaling

1 Introduction

A mathematical model is a representation of a physical system, often underpinned by scientific theory, which is used to understand, predict and control the physical system. When such models are evaluated by complex, computationally expensive code, they are known as computer models.

A mathematical model is considered to be a function taking certain arguments and returning a theoretical prediction of a feature (or features) of the physical system. Following Plumlee (2017), the arguments to the mathematical model can be split into two groups. They are (a) *general inputs*: controllable or measurable variables of the system; and (b) *calibration parameters*: unknown characteristics of the physical system that cannot be controlled or directly measured.

This paper addresses calibration: the task of attributing values to the calibration parameters using observations of the physical system. The values given to the calibration parameters should, in some senses, result in the mathematical model (when considered solely as a function of the general inputs) being “close” to the physical system. This goal implicitly recognises that the mathematical model is an incomplete (or inexact) representation of the physical system, i.e. there do not exist values of the calibration parameters such that the mathematical model is equal to the physical system for all values of the general inputs.

In their seminal work on calibration, Kennedy and O’Hagan (2001) considered the bias function, i.e. the difference between the physical system and the mathematical model. Since the bias function is unknown, a Gaussian process prior distribution is assumed for this function. A Bayesian approach is then adopted with the goal of evaluating the marginal posterior distribution of the calibration parameters. However, Tuo and Wu (2016) show that the actual parameter values that the Kennedy and O’Hagan approach are estimating depend on the Gaussian process prior for the bias function and this dependence does not diminish as the number of observations of the physical system grows. To address this problem, Tuo and Wu (2015) proposed an alternative (frequentist) framework for calibration. They define values of the calibration parameters that minimise the squared norm of the bias function (in the associated L^2 space). Estimating these values is now the target of the Tuo and Wu (2015) framework. This is achieved by minimising a loss function given by a non-parametric estimate of the squared L^2 norm of the bias function, formed using the observations of the physical system. Under certain assumptions, the resulting estimator is consistent for the target calibration parameter values. An alternative approach to calibrating a mathematical model is ordinary least squares (OLS). Under differing conditions, Tuo and Wu (2015) and Wong et al. (2017) show that the parameter values minimising the OLS loss will converge to the target parameter values under L^2 calibration.

Due to the natural way that Bayesian inference manages uncertainty quantification, several authors have recently proposed Bayesian analogues of the Tuo and Wu (2015) L^2 calibration framework. Plumlee (2017) modifies the Kennedy and O’Hagan (2001) framework by, first, noting that minimising the squared L^2 norm of the bias function imposes orthogonality of the bias function and the gradient of the mathematical model. This orthogonality places constraints on the Gaussian process prior for the bias function. Gu and Wang (2018) pointed out that orthogonality of the bias and mathematical model gradient is a necessary, but not sufficient condition, for minimising the squared L^2 norm. Instead, they assumed a prior distribution on the squared L^2 norm penalising “large” bias functions. Xie and Xu (2021) proposed a different approach whereby a Gaussian process prior for the physical system is assumed which is updated to a Gaussian process posterior in light of observations of the physical system. Then, minimising the squared L^2 norm induces a posterior distribution on the calibration parameters.

This paper proposes a general Bayesian (e.g. Bissiri et al., 2016) framework for L^2 calibration of mathematical models. Under this approach, unlike traditional Bayesian inference, a so-called generalised posterior distribution for the calibration parameters can be formed using the L^2 and OLS losses without needing to specify a probabilistic data-generating process for the observations of the physical system.

The advantages of the general Bayesian framework, when compared with existing traditional Bayesian calibration approaches, are that it is conceptually and computationally simpler, allows more transparent incorporation of prior information, and, as stated above, does not require the specification of a probabilistic data-generating process for the observations. The benefit of the last advantage is that the inference should be less sensitive to the misspecification of the data-generating process.

However, as will be seen, the major impediment to implementing general Bayesian L^2 calibration is that the scale of the generalised posterior is essentially arbitrary. To address this problem, automatic, computationally simple, scalings of the L^2 and OLS losses are developed. These scalings are designed to match asymptotic properties of the generalised posterior with corresponding frequentist properties of the L^2 and OLS estimators.

The remainder of this paper is organised as follows. Section 2 provides a more in depth description of existing approaches to calibration and general Bayesian inference. Section 3 develops automatic scalings for the L^2 and OLS losses. Section 4 considers the asymptotic properties of the generalised Bayesian distributions under the L^2 and OLS losses. Section 5 discusses the practical implementation of the approach. Finally, in Section 6 we implement the methodology on illustrative and real examples.

2 Background

In this section, we provide a mathematical description of the calibration of mathematical models (Section 2.1), and brief outlines of existing related approaches to calibration (Section 2.2) and general Bayesian inference (Section 2.3).

2.1 Setup

In this sub-section, we provide a mathematical description to the problem of the calibration of mathematical models. Let $\eta(\mathbf{x}, \boldsymbol{\theta})$ denote the mathematical model where $\mathbf{x} = (x_1, \dots, x_k)^\top \in \mathcal{X}$ denotes the $k \times 1$ vector of general inputs with $\mathcal{X} \subset \mathbb{R}^k$ the input space and $\boldsymbol{\theta} = (\theta_1, \dots, \theta_p)^\top \in \Theta \subset \mathbb{R}^p$ denotes the $p \times 1$ vector of unknown calibration parameters. In this paper, we assume, perhaps after transformation, that $\mathcal{X} = [0, 1]^k$ with $\text{Vol}(\mathcal{X}) = \int_{\mathcal{X}} d\mathbf{x} = 1$.

Calibration is performed using n observations of the physical system. That is, for $i = 1, \dots, n$, a response y_i is observed of the physical system under inputs $\mathbf{x}_i = (x_{i1}, \dots, x_{ik})^\top \in \mathcal{X}$. Let $\mathbf{y} = (y_1, \dots, y_n)^\top$ be the $n \times 1$ vector of responses and let $\mathbf{X} = \{\mathbf{x}_1, \dots, \mathbf{x}_n\}$ be the design. Initially, the design can either be fixed or the realisation of a random variable. However, later, we focus on the case where the design is fixed.

It is assumed that the true data-generating process for \mathbf{y} is

$$y_i = \mu(\mathbf{x}_i) + e_i \tag{1}$$

for $i = 1, \dots, n$, where $\mu(\mathbf{x})$ is a function giving the true value of the physical system at inputs \mathbf{x} , and e_1, \dots, e_n are independent and identically distributed random variables with $E(e_i) = 0$ and $\text{var}(e_i) = \sigma^2 > 0$ representing observational error.

As discussed in Section 1, the challenge of calibration is that the mathematical model is inexact, i.e. there do not exist values of the calibration parameters $\boldsymbol{\theta}_0 \in \mathbb{R}^p$ such that $\eta(\mathbf{x}, \boldsymbol{\theta}_0) = \mu(\mathbf{x})$ for all $\mathbf{x} \in \mathcal{X}$. Instead, calibration aims to find $\boldsymbol{\theta}_C \in \Theta$ such that $\eta(\mathbf{x}, \boldsymbol{\theta}_C)$ is “close” to $\mu(\mathbf{x})$ for all $\mathbf{x} \in \mathcal{X}$.

2.2 Existing related approaches to calibration

2.2.1 Kennedy and O'Hagan calibration

Under the Kennedy and O'Hagan (2001) framework it is assumed that the i th observational error has $e_i \sim N(0, \tau^2)$, for $i = 1, \dots, n$, and

$$\mu(\mathbf{x}) = \eta(\mathbf{x}, \boldsymbol{\theta}_C) + \delta(\mathbf{x}),$$

where $\delta(\mathbf{x})$ is an unknown bias function giving the difference between the true physical system and the mathematical model. Kennedy and O'Hagan (2001) imposed a zero-mean Gaussian process prior distribution for the bias function, i.e. $\delta(\cdot) \sim GP[0, \chi(\cdot, \cdot; \boldsymbol{\psi})]$ where $\chi(\cdot, \cdot; \boldsymbol{\psi})$ is a specified covariance function depending on unknown parameters $\boldsymbol{\psi}$. A fully Bayesian approach is then taken by evaluating the marginal posterior distribution of $\boldsymbol{\theta}_C$, conditional on observations of the physical system, after specifying a joint prior distribution for $\boldsymbol{\theta}_C$, τ^2 and $\boldsymbol{\psi}$.

A key question is what do the values of $\boldsymbol{\theta}_C$ actually represent? We address this question for the fully Bayesian analysis in Section 2.4. However, beforehand, in a simplified setting where $\tau^2 = 0$, and the values of $\boldsymbol{\psi}$ are assumed known, Tuo and Wu (2016) show that the maximum likelihood estimator of $\boldsymbol{\theta}_C$ converges to $\boldsymbol{\theta}_{KOH}$; the values of $\boldsymbol{\theta}$ that minimise the squared norm of $\delta(\mathbf{x})$ in the associated reproducing kernel Hilbert space (RKHS; e.g. Lange 2010, Section 17.5) with kernel χ , denoted $\mathcal{H}_\chi(\mathcal{X})$. The convergence of the estimator of $\boldsymbol{\theta}_C$ to quantities depending on the choice of covariance function has been criticised by several authors (e.g. Tuo and Wu, 2015, 2016; Plumlee, 2017; Wong et al., 2017).

2.2.2 Frequentist L^2 and OLS calibration

To address the asymptotic covariance function dependence of the Kennedy and O'Hagan (2001) framework, Tuo and Wu (2015) defined $\boldsymbol{\theta}_C$ to be $\boldsymbol{\theta}_{L^2}$; the values of $\boldsymbol{\theta}$ that minimise the squared norm of the bias function in the associated L^2 space, i.e.

$$\boldsymbol{\theta}_{L^2} = \arg \min_{\boldsymbol{\theta} \in \mathbb{R}^p} L_{L^2}(\boldsymbol{\theta}),$$

where

$$\begin{aligned} L_{L^2}(\boldsymbol{\theta}) &= \int_{\mathcal{X}} (\mu(\mathbf{x}) - \eta(\mathbf{x}, \boldsymbol{\theta}))^2 d\mathbf{x} \\ &= \|\mu(\cdot) - \eta(\cdot, \boldsymbol{\theta})\|_{L^2(\mathcal{X})}^2. \end{aligned} \tag{2}$$

They then define the estimators $\hat{\boldsymbol{\theta}}_{L^2}$ of $\boldsymbol{\theta}$ to be

$$\hat{\boldsymbol{\theta}}_{L^2} = \arg \min_{\boldsymbol{\theta} \in \Theta} \ell_{L^2}(\boldsymbol{\theta}; \mathbf{y}),$$

where

$$\begin{aligned} \ell_{L^2}(\boldsymbol{\theta}; \mathbf{y}) &= \int_{\mathcal{X}} (\hat{\mu}(\mathbf{x}) - \eta(\mathbf{x}, \boldsymbol{\theta}))^2 d\mathbf{x}, \\ &= \|\hat{\mu}(\cdot) - \eta(\cdot, \boldsymbol{\theta})\|_{L^2(\mathcal{X})}^2, \end{aligned} \tag{3}$$

is termed the L^2 loss and $\hat{\mu}(\mathbf{x})$ is a non-parametric estimate of $\mu(\mathbf{x})$ formed from the observations of the physical system. Specifically,

$$\hat{\mu} = \arg \min_{\mu \in \mathcal{F}} R(\mu),$$

where

$$R(\mu) = \sum_{i=1}^n (y_i - \mu(\mathbf{x}_i))^2 + J(\mu),$$

\mathcal{F} is a space of functions, and $J(\mu)$ is a penalty on the complexity of μ . Let $\kappa(\cdot, \cdot; \rho)$ be a covariance function depending on parameters ρ and suppose $\mathcal{F} = \mathcal{H}_\kappa(\mathcal{X})$ and

$$J(\mu) = \lambda \|\mu\|_{\mathcal{H}_\kappa(\mathcal{X})},$$

where $\|\cdot\|_{\mathcal{H}_\kappa(\mathcal{X})}$ is the RKHS norm with kernel. Then it can be shown (e.g. Wahba, 1990) that $\hat{\mu}(\mathbf{x})$ is given by

$$\hat{\mu}(\mathbf{x}) = \sum_{i=1}^n s_i(\mathbf{x}) y_i, \quad (4)$$

where $\mathbf{s}(\mathbf{x}) = (s_1(\mathbf{x}), \dots, s_n(\mathbf{x}))^\top$ is

$$\mathbf{s}(\mathbf{x}) = \Phi^{-1} \mathbf{k}(\mathbf{x}). \quad (5)$$

In (5), $\mathbf{k}(\mathbf{x}) = (\kappa(\mathbf{x}, \mathbf{x}_1; \rho), \dots, \kappa(\mathbf{x}, \mathbf{x}_n; \rho))^\top$ and $\Phi = I_n + K$, where I_n is the $n \times n$ identity matrix and K is the $n \times n$ matrix with ij th element $\kappa(\mathbf{x}_i, \mathbf{x}_j; \rho)$. The values of ρ can be estimated via generalised cross-validation, i.e. let S be the $n \times n$ matrix with i th row given by $\mathbf{s}(\mathbf{x}_i)$, then

$$\hat{\rho} = \arg \min \frac{\mathbf{y}^\top (I_n - S)^2 \mathbf{y}}{(1 - \text{tr}(S)/n)^2}.$$

Under certain regularity conditions, the most stringent of which is that the elements, $\{\mathbf{x}_1, \dots, \mathbf{x}_n\}$, of \mathbf{X} are realisations of independent and identically distributed random variables from the uniform distribution over \mathcal{X} , Tuo and Wu (2015) show that $\hat{\theta}_{L^2}$ is a consistent estimator of θ_{L^2} . Furthermore, $\hat{\theta}_{L^2}$ has the following asymptotic normal distribution

$$\hat{\theta}_{L^2} \sim N \left(\theta_{L^2}, \frac{1}{n} V^{-1} W_{L^2:U} V^{-1} \right), \quad (6)$$

where

$$V = \frac{\partial^2 L_{L^2}(\theta_{L^2})}{\partial \theta \partial \theta^\top} \quad (7)$$

$$W_{L^2:U} = 4\sigma^2 \int_{\mathcal{X}} \frac{\partial \eta(\mathbf{x}, \theta_{L^2})}{\partial \theta} \frac{\partial \eta(\mathbf{x}, \theta_{L^2})}{\partial \theta^\top} d\mathbf{x}. \quad (8)$$

For clarity, note that consistency and the asymptotic distribution (6) follow from marginalising over \mathbf{y} and \mathbf{X} , i.e. the results are not conditional on the design. In (8), the U in the subscript $L^2 : U$ indicates that the elements of the design are realisations of a uniform random variable on \mathcal{X} .

Alternatively, Tuo and Wu (2015) considered the ordinary least squares estimator given by

$$\hat{\theta}_{OLS} = \arg \min_{\theta \in \Theta} \ell_{OLS}(\theta; \mathbf{y}),$$

where

$$\ell_{OLS}(\theta; \mathbf{y}) = \frac{1}{n} \sum_{i=1}^n (y_i - \eta(\mathbf{x}_i, \theta))^2$$

is the *OLS loss*. Under the same requirement that the elements of \mathbf{X} be a random sample from the uniform distribution over \mathcal{X} , Tuo and Wu (2015) show that $\hat{\theta}_{OLS}$ is a consistent estimator of θ_{L^2} . Furthermore, $\hat{\theta}_{OLS}$ has the following asymptotic normal distribution

$$\hat{\theta}_{OLS} \sim N \left(\theta_{L^2}, \frac{1}{n} V^{-1} W_{OLS:U} V^{-1} \right),$$

where

$$W_{OLS:U} = 4 \int_{\mathcal{X}} \left[\sigma^2 + (\mu(\mathbf{x}) - \eta(\mathbf{x}, \boldsymbol{\theta}_{L^2}))^2 \right] \frac{\partial \eta(\mathbf{x}, \boldsymbol{\theta}_{L^2})}{\partial \boldsymbol{\theta}} \frac{\partial \eta(\mathbf{x}, \boldsymbol{\theta}_{L^2})}{\partial \boldsymbol{\theta}^T} d\mathbf{x}. \quad (9)$$

In (9), the U in the subscript $OLS : U$ indicates that the elements of the design are realisations of a uniform random variable on \mathcal{X} . Tuo and Wu (2015) observed that the asymptotic variance of $\hat{\boldsymbol{\theta}}_{OLS}$ is larger than for $\hat{\boldsymbol{\theta}}_{TW}$, i.e. $W_{OLS:U} \succcurlyeq W_{L^2:U}$, where $A \succcurlyeq B$, means that $A - B$ is positive-semi-definite. Moreover, equality is only achieved when there exist $\boldsymbol{\theta}_0$ such that $\mu(\mathbf{x}) = \eta(\mathbf{x}, \boldsymbol{\theta}_0)$ for all $\mathbf{x} \in \mathcal{X}$, i.e. the mathematical model is exact.

However, there are several advantages to frequentist OLS calibration. It is computationally less demanding since the integration required to evaluate $\ell_{L^2}(\boldsymbol{\theta}; \mathbf{y})$ is rarely available in closed form and requires numerical evaluation. Additionally, for the non-parametric regression, the values of $\boldsymbol{\rho}$ need to be determined.

Wong et al. (2017) studied frequentist OLS calibration under a fixed, non-random design. Under certain conditions, they showed, among other properties, that $\hat{\boldsymbol{\theta}}_{OLS}$ are consistent estimators of $\boldsymbol{\theta}_{L^2}$. We take advantage of their results in Section 3.

2.2.3 Bayesian L^2 calibration approaches

Bayesian approaches allow a coherent approach to uncertainty quantification. Due to this, several authors have recently proposed Bayesian L^2 calibration approaches.

Consider the definition of $\boldsymbol{\theta}_{L^2}$ as the values of $\boldsymbol{\theta}$ minimising $L_{L^2}(\boldsymbol{\theta})$ given by (2). This implies that $\partial L_{L^2}(\boldsymbol{\theta}_{L^2})/\partial \boldsymbol{\theta} = \mathbf{0}$, where

$$\frac{\partial L_{L^2}(\boldsymbol{\theta})}{\partial \boldsymbol{\theta}} = -2 \int_{\mathcal{X}} \frac{\partial \eta(\boldsymbol{\theta}, \mathbf{x})}{\partial \boldsymbol{\theta}} (\mu(\mathbf{x}) - \eta(\mathbf{x}, \boldsymbol{\theta})) d\mathbf{x} = \left\langle \frac{\partial \eta(\cdot, \boldsymbol{\theta})}{\partial \boldsymbol{\theta}}, \mu(\cdot) - \eta(\cdot, \boldsymbol{\theta}) \right\rangle_{L^2(\mathcal{X})},$$

with $\langle \cdot, \cdot \rangle_{L^2(\mathcal{X})}$ denoting the L^2 inner product on \mathcal{X} . Therefore, the bias function is orthogonal to the gradient (with respect to $\boldsymbol{\theta}$) of the mathematical model, at $\boldsymbol{\theta} = \boldsymbol{\theta}_{L^2}$. Under the Kennedy and O'Hagan (2001) framework, this orthogonality condition introduces constraints on the Gaussian process prior for the bias function, i.e. it modifies the form of the chosen correlation function χ . Imposition of these constraints leads to the Plumlee (2017) Bayesian L^2 calibration approach.

However, due to the potential existence of local minima, the orthogonality condition can be true for values of $\boldsymbol{\theta}$ not equal to $\boldsymbol{\theta}_{L^2}$. For this reason, Gu and Wang (2018) assumed a prior distribution for $L_{L^2}(\boldsymbol{\theta})$, in addition to the Kennedy and O'Hagan Gaussian process prior on the bias function, which penalises large values of the bias function.

An alternative approach proposed by Xie and Xu (2021) begins by assuming a zero mean Gaussian process for $\mu(\mathbf{x})$, i.e. $\mu(\cdot) \sim \text{GP}[0, \kappa(\cdot, \cdot; \boldsymbol{\rho})]$. The resulting posterior distribution for $\mu(\mathbf{x})$ is a normal distribution with mean $\hat{\mu}(\mathbf{x})$ given by (4) and variance $\nu(\mathbf{x}) = \kappa(\mathbf{x}, \mathbf{x}; \boldsymbol{\rho}) - \mathbf{k}(\mathbf{x})^T \mathbf{s}(\mathbf{x})$. By writing $L_{L^2}(\boldsymbol{\theta})$ as a functional of $\mu(\mathbf{x})$, i.e.

$$L[\boldsymbol{\theta}, \mu(\mathbf{x})] = \int_{\mathcal{X}} (\mu(\mathbf{x}) - \eta(\boldsymbol{\theta}, \mathbf{x}))^2 d\mathbf{x},$$

Xie and Xu (2021) noted that this induces a posterior distribution for $L_{L^2}[\boldsymbol{\theta}, \mu(\mathbf{x})]$ and hence for the values of $\boldsymbol{\theta}$ minimising $L_{L^2}[\boldsymbol{\theta}, \mu(\mathbf{x})]$. Xie and Xu (2021) proved, under certain conditions; 1) the resulting posterior distribution converges to a point mass at $\boldsymbol{\theta}_{L^2}$ and 2) a limiting normal distribution applies.

2.3 General Bayesian Inference

We now provide a brief outline of general Bayesian inference for calibrating a mathematical model. General Bayesian inference begins with the specification of a loss function denoted $\ell(\boldsymbol{\theta}; \mathbf{y})$. This function identifies desirable values for the calibration parameters based on observations \mathbf{y} . Let $\boldsymbol{\theta}_\ell = \arg \min_{\boldsymbol{\theta} \in \Theta} L(\boldsymbol{\theta})$ where $L(\boldsymbol{\theta}) = \mathbb{E}_{\mathbf{y}} [\ell(\boldsymbol{\theta}; \mathbf{y})]$ is the expected loss under the true probability distribution of the observations \mathbf{y} , i.e. under (1). It is assumed that learning about the values of $\boldsymbol{\theta}_\ell$ is the target of the inference. Ultimately, we aim to set $\boldsymbol{\theta}_\ell = \boldsymbol{\theta}_{L^2}$, at least asymptotically.

General Bayesian inference proceeds via the generalised (or Gibbs) posterior distribution given by

$$\pi_G(\boldsymbol{\theta} | \mathbf{y}) \propto \exp[-n\ell(\boldsymbol{\theta}; \mathbf{y})] \pi(\boldsymbol{\theta}), \quad (10)$$

where $\pi(\boldsymbol{\theta})$ is the probability density function (pdf) of the prior distribution for $\boldsymbol{\theta}_\ell$ and $\pi_G(\mathbf{y} | \boldsymbol{\theta}) = \exp[-n\ell(\boldsymbol{\theta}; \mathbf{y})]$ is known as the *generalised likelihood*. Bissiri et al. (2016) show that the generalised posterior distribution provides a coherent representation of subjective uncertainty about the values of $\boldsymbol{\theta}_\ell$.

Note that the traditional Bayesian posterior distribution can be viewed as a general Bayesian posterior under the *self-information loss* $\ell_{SI}(\boldsymbol{\theta}; \mathbf{y}) = -\frac{1}{n} \log \pi(\mathbf{y} | \boldsymbol{\theta})$, where $\pi(\mathbf{y} | \boldsymbol{\theta})$ is the likelihood function. The likelihood function follows from the specification of the data-generating process for the observations \mathbf{y} . Under the self-information loss, the target parameters $\boldsymbol{\theta}_{SI}$ are those values of $\boldsymbol{\theta}$ that minimise

$$L_{SI}(\boldsymbol{\theta}) = \mathbb{E}_{\mathbf{y}} [\ell_{SI}(\boldsymbol{\theta}; \mathbf{y})] = -\frac{1}{n} \mathbb{E}_{\mathbf{y}} [\log \pi(\mathbf{y} | \boldsymbol{\theta})].$$

It follows that $\boldsymbol{\theta}_{SI}$ minimise the Kullback-Liebler divergence between the distribution assumed for \mathbf{y} by the model and the true distribution. Regardless of whether the mathematical model is exact or not, the standard Bayesian posterior provides coherent inference for $\boldsymbol{\theta}_{SI}$.

Let us analyse the Kennedy and O'Hagan (2001) framework under this knowledge. Extend the parameters to include the nuisance parameters $\boldsymbol{\psi}$ and τ^2 . Then the loss is

$$\ell_{SI}(\boldsymbol{\theta}, \tau^2, \boldsymbol{\psi}; \mathbf{y}) = -\frac{1}{n} \log \pi(\mathbf{y} | \boldsymbol{\theta}, \tau^2, \boldsymbol{\psi}),$$

where the log-likelihood is

$$\log \pi(\mathbf{y} | \boldsymbol{\theta}, \tau^2, \boldsymbol{\psi}) = -\frac{n}{2} \log(2\pi) - \frac{1}{2} \log |R| - \frac{1}{2} [\mathbf{y} - \boldsymbol{\eta}(\boldsymbol{\theta})]^T R^{-1} (\mathbf{y} - \boldsymbol{\eta}(\boldsymbol{\theta})). \quad (11)$$

In (11), $\boldsymbol{\eta}(\boldsymbol{\theta}) = (\eta(\mathbf{x}_1, \boldsymbol{\theta}), \dots, \eta(\mathbf{x}_n, \boldsymbol{\theta}))^T$ and R is an $n \times n$ matrix with ij th element

$$R_{ij} = \tau^2 I(\mathbf{x}_i = \mathbf{x}_j) + \chi(\mathbf{x}_i, \mathbf{x}_j; \boldsymbol{\psi}),$$

with $I(A)$ the indicator function for event A . The expected loss is then

$$\begin{aligned} L_{SI}(\boldsymbol{\theta}, \tau^2, \boldsymbol{\psi}) &= -\frac{1}{n} \mathbb{E}_{\mathbf{y}} [\log \pi(\mathbf{y} | \boldsymbol{\theta}, \tau^2, \boldsymbol{\psi})] \\ &= \frac{1}{2} \log(2\pi) + \frac{1}{2n} \log |R| + \frac{1}{2n} [\boldsymbol{\mu} - \boldsymbol{\eta}(\boldsymbol{\theta})]^T R^{-1} [\boldsymbol{\mu} - \boldsymbol{\eta}(\boldsymbol{\theta})] + \frac{\sigma^2}{2n} \text{tr}(R^{-1}). \end{aligned}$$

Therefore the target calibration parameters under the full Kennedy and O'Hagan (2001) framework are

$$\boldsymbol{\theta}_{KOH:SI} = \arg \min_{\boldsymbol{\theta} \in \Theta} [\boldsymbol{\mu} - \boldsymbol{\eta}(\boldsymbol{\theta})]^T R^{-1} [\boldsymbol{\mu} - \boldsymbol{\eta}(\boldsymbol{\theta})].$$

Under the simplified Kennedy and O'Hagan calibration considered by Tuo and Wu (2016), $\boldsymbol{\theta}_{KOH:SI}$ are the maximum likelihood estimators of the calibration parameters. Tuo and Wu (2016, Theorem 1) showed that $\boldsymbol{\theta}_{KOH:SI}$ converge to $\boldsymbol{\theta}_{KOH}$, the values of the calibration parameters that minimise the RKHS norm with kernel χ , as the design points become dense on \mathcal{X} . Therefore, the target parameters of the fully Bayesian Kennedy and O'Hagan calibration are intrinsically linked with the choice of kernel function $\chi(\cdot, \cdot; \boldsymbol{\psi})$.

2.4 The idea

The purpose of this paper is to build a general Bayesian framework for the calibration of mathematical models using the L^2 and OLS loss functions described in Section 2.2.2. The major hurdle when performing general Bayesian inference is that the scale of the generalised likelihood compared to the prior distribution is arbitrary. For example, consider a loss function given by $\gamma\ell_{L^2}(\boldsymbol{\theta}; \mathbf{y})$, for some specified constant $\gamma > 0$, independent of $\boldsymbol{\theta}$. The values of $\boldsymbol{\theta}$ that maximise the generalised likelihood are the same as those that minimise the loss function and these are not changed by varying γ . Neither are the target parameter values that minimise the expected loss. However, varying γ does change the generalised posterior distribution, both in terms of location and scale. Consider the extreme cases. As $\gamma \rightarrow 0$, the generalised posterior will converge to the prior distribution. Conversely, as $\gamma \rightarrow \infty$, the generalised posterior will converge to a point mass at $\hat{\theta}_{L^2}$.

To illustrate, consider the following example modified from Plumlee (2017). The mathematical model is

$$\eta(x, \theta) = \theta x$$

with $x \in \mathcal{X} = [0, 1]$ and $p = k = 1$. The physical process is assumed known and is given by $\mu(x) = 4x + x \sin(5x)$. In this case, θ_{L^2} can be calculated in closed form as

$$\theta_{L^2} = \frac{\int_0^1 x(4x + x \sin(5x))dx}{\int_0^1 x^2 dx} = 3.5653.$$

This is slightly different to the value of 3.5609 reported by Plumlee (2017) and Xie and Xu (2021).

We simulate $n = 6$ values via $y_i = \mu(x_i) + e_i$, for $i = 1, \dots, n$, where x_1, \dots, x_n are equally-spaced on \mathcal{X} and $e_i \stackrel{\text{iid}}{\sim} N(0, \sigma^2)$ with $\sigma^2 = 0.02^2$. Figure 1(a) shows the responses plotted against the inputs. Also shown are the functions $\mu(x)$ and $\hat{\mu}(x)$ plotted against x . Under these responses, the frequentist estimates are $\hat{\theta}_{L^2} = 3.636$ and $\hat{\theta}_{OLS} = 3.449$.

Figure 1(b) shows the generalised posterior densities under L^2 and OLS calibration for two different values of γ , namely $\gamma = 1$ and $\gamma = 500$. In all cases, following Plumlee (2017), we have assumed a prior distribution where $\theta_{L^2} \sim N(0, 1)$. In Figure 1(b), the true value of θ_{L^2} is identified by the vertical dotted line. When $\gamma = 500$, both distributions have very low posterior density at θ_{L^2} . The generalised posterior means for L^2 and OLS are 3.634 and 3.447, respectively, i.e. close to the frequentist estimates. Conversely, when $\gamma = 1$, both distributions have high uncertainty. The corresponding posterior means are 2.932 and 2.840, respectively, i.e. shrunk towards the prior mean of 0.

In Section 3 methods are developed to automatically scale the loss function, e.g. to automatically specify γ . This is accomplished so that certain frequentist properties are maintained, specifically the asymptotic expectation and distribution of an analogue of the likelihood ratio statistic.

3 Automatic scaling of the generalised posterior distribution

3.1 Introduction

As discussed in Section 2.4, the scaling of the loss function is crucial. In this section, we propose automatic scaling procedures adapted from the composite likelihood literature (Pauli et al., 2011; Ribatet et al., 2012).

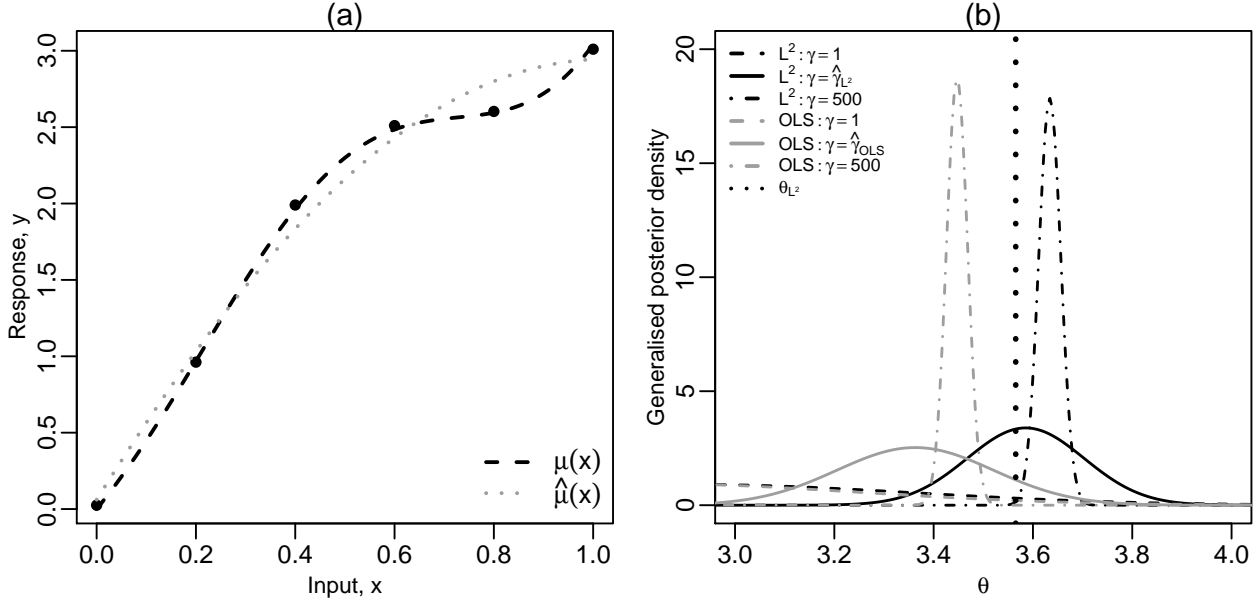


Figure 1: (a) Responses, y_1, \dots, y_n plotted against the inputs x_1, \dots, x_n , and the functions $\mu(x)$ and $\hat{\mu}(x)$ plotted against x . (b) Generalised posterior densities plotted against θ , under the L^2 and OLS loss functions for differing values of γ . The true value of $\theta_{L^2} = 3.5653$ is indicated by the vertical dotted line.

Initially, suppose the mathematical model is exact. Then there exist $\boldsymbol{\theta}_0$ such that $\eta(\mathbf{x}, \boldsymbol{\theta}_0) = \mu(\mathbf{x})$ for all $\mathbf{x} \in \mathcal{X}$. Furthermore, suppose under (1) that the joint distribution of the errors e_1, \dots, e_n is completely specified and does not depend on any unknown nuisance parameters. The likelihood ratio statistic is

$$\Lambda_0(\boldsymbol{\theta}_0; \mathbf{y}, \mathbf{X}) = 2 \left(\log \pi(\mathbf{y}|\hat{\boldsymbol{\theta}}) - \log \pi(\mathbf{y}|\boldsymbol{\theta}_0) \right),$$

where $\hat{\boldsymbol{\theta}}$ are the maximum likelihood estimators of $\boldsymbol{\theta}_0$. Under certain regularity conditions, $\Lambda_0(\boldsymbol{\theta}_0; \mathbf{y}, \mathbf{X})$ converges in distribution to χ_p^2 as $n \rightarrow \infty$, and, in particular, $\mathbb{E}[\Lambda_0(\boldsymbol{\theta}_0; \mathbf{y}, \mathbf{X})] \rightarrow p$.

Recall, from Section 2.3, the self-information loss is $\ell_{SI}(\boldsymbol{\theta}; \mathbf{y}) = -n^{-1} \log \pi(\mathbf{y}|\boldsymbol{\theta})$. Then the likelihood ratio statistic can be written

$$\Lambda_0(\boldsymbol{\theta}_0; \mathbf{y}) = 2n \left[\ell_{SI}(\boldsymbol{\theta}_0; \mathbf{y}) - \ell_{SI}(\hat{\boldsymbol{\theta}}; \mathbf{y}) \right]. \quad (12)$$

The idea is to choose the scaling of the loss so that, when replacing ℓ_{SI} and $\hat{\boldsymbol{\theta}}$ in (12) by the chosen scaled loss and the frequentist estimators, respectively, asymptotic properties of the resulting Λ are maintained as those of Λ_0 . In particular, *magnitude scaling* ensures that the asymptotic expectation of Λ is equal to p . By contrast, *curvature scaling* ensures that Λ converges in distribution to χ_p^2 . These procedures are described in Section 3.4.

However, the first step is to establish necessary results on frequentist calibration under the L^2 and OLS loss functions. Similar to Wong et al. (2017), we consider the design $\mathbf{X} = \{\mathbf{x}_1, \dots, \mathbf{x}_n\}$ to be fixed. For the L^2 loss, we assume that the elements of $\boldsymbol{\rho}$ (the parameters controlling the covariance function κ) are fixed.

To begin we require the following conditions common to both L^2 and OLS loss functions. Define $B_\epsilon(\mathbf{u}) = \{\mathbf{u} \in \Theta : \mathbf{u}^T \mathbf{u} < \epsilon\}$ and $r_n(\mathbf{u})$ to be a function where there exist $\epsilon_0, c_0 > 0$ such that for n sufficiently large, $|r_n(\mathbf{u})| \leq c_0 (\mathbf{u}^T \mathbf{u})^{3/2}$ for $\mathbf{u} \in B_{\epsilon_0}(\mathbf{0})$.

C1 The errors e_1, \dots, e_n are independent and identically distributed with $E_{e_i}(e_i) = 0$ and $\text{var}_{e_i}(e_i) = \sigma^2 < \infty$.

C2 Θ is a compact subset of \mathbb{R}^p .

C3 \mathcal{X} is a convex and closed subset of \mathbb{R}^k .

C4 $\hat{\boldsymbol{\theta}}_{L^2} = \arg \min_{\boldsymbol{\theta} \in \mathbb{R}^p} L_{L^2}(\boldsymbol{\theta}) \in E$ are unique and where E is an open, convex and bounded subset of Θ .

C5 V is positive-definite, where V is defined in (7).

C6 For $u, v = 1, \dots, p$, $\partial \eta(\mathbf{x}, \boldsymbol{\theta}) / \partial \theta_u$ and $\partial^2 \eta(\mathbf{x}, \boldsymbol{\theta}) / \partial \theta_u \partial \theta_v$ are continuous with respect to \mathbf{x} for $\boldsymbol{\theta} \in B_\epsilon(\hat{\boldsymbol{\theta}}_{L^2})$.

3.2 Properties of frequentist L^2 calibration

In this section we establish properties of frequentist L^2 calibration, namely consistency, convergence of the second derivative of the loss, and a second-order Taylor series representation of the loss. Beforehand we state required conditions for L^2 calibration.

L1 $\hat{\boldsymbol{\theta}}_{L^2} \in E$ (where E is defined in C4) and are unique.

L2 $\ell_{L^2}(\boldsymbol{\theta}; \mathbf{y})$ has continuous and uniformly bounded third derivatives (with respect to $\boldsymbol{\theta}$).

L3 $\sup_{\boldsymbol{\theta} \in \Theta} \|\eta(\cdot, \boldsymbol{\theta})\|_{L^2} < \infty$.

L4 $\hat{\mu}(\mathbf{x}) \xrightarrow{p} \mu(\mathbf{x})$ for all $\mathbf{x} \in \mathcal{X}$.

L5 $\|\hat{\mu}(\cdot)\|_{L^2(\mathcal{X})} = O_p(1)$.

L6 There exists an $M < \infty$ such that $|\mu(\mathbf{x})| < M$ for all $\mathbf{x} \in \mathcal{X}$.

L7 There exists a $t > 0$ such that $E(|e_i|^{2+t}) < \infty$ and

$$\frac{\sum_{i=1}^n |s_i(\mathbf{x})|^{2+t}}{\left[\sum_{i=1}^n s_i(\mathbf{x})^2\right]^{1+t/2}} \rightarrow 0,$$

as $n \rightarrow \infty$, for all $\mathbf{x} \in \mathcal{X}$, where $s_1(\mathbf{x}), \dots, s_n(\mathbf{x})$ are the elements of $\mathbf{s}(\mathbf{x})$ defined in (5).

Consider condition L4, stating that the non-parametric smoother $\hat{\mu}(\mathbf{x})$ converges (in probability) to $\mu(\mathbf{x})$. Georgiev (1988, Theorem 2) showed that, for a fixed design, condition L4 is ensured by the assumption of C1, C3, L6 and the following condition.

L8 The design points $\mathbf{x}_1, \dots, \mathbf{x}_n$ are chosen such that

- (a) $\sum_{i=1}^n s_i(\mathbf{x}) \rightarrow 1$ as $n \rightarrow \infty$ for all $\mathbf{x} \in \mathcal{X}$;
- (b) $\sup_{i=1, \dots, n} |s_i(\mathbf{x})| = O(n^{-1})$ for all $\mathbf{x} \in \mathcal{X}$;
- (c) $\sum_{i=1}^n |s_i(\mathbf{x})| \leq D$ for some $D < \infty$ for all n and $\mathbf{x} \in \mathcal{X}$; and
- (d) $\sum_{i=1}^n |s_i(\mathbf{x})| I \left[(\mathbf{x}_i - \mathbf{x})^T (\mathbf{x}_i - \mathbf{x}) > a \right] \rightarrow 0$ as $n \rightarrow \infty$ for all $a > 0$.

The following lemma provides the required asymptotic results for frequentist L^2 calibration.

Lemma 1 (Frequentist L^2 calibration)

Under conditions C1-C6 and L1-L7, the following statements are true.

(a) As $n \rightarrow \infty$, then $\hat{\boldsymbol{\theta}}_{L^2} \xrightarrow{p} \boldsymbol{\theta}_{L^2}$.

(b) As $n \rightarrow \infty$, then, $\frac{\partial^2 \ell_{L^2}(\boldsymbol{\theta}_{L^2}; \mathbf{y})}{\partial \boldsymbol{\theta} \partial \boldsymbol{\theta}^T} \xrightarrow{p} V$.

(c) The L^2 loss can be written

$$\ell_{L^2}(\boldsymbol{\theta}; \mathbf{y}) = \ell_{L^2}(\hat{\boldsymbol{\theta}}_{L^2}; \mathbf{y}) + \frac{1}{2} \left(\boldsymbol{\theta} - \hat{\boldsymbol{\theta}}_{L^2} \right)^T \hat{V}_{L^2} \left(\boldsymbol{\theta} - \hat{\boldsymbol{\theta}}_{L^2} \right) + r_n \left(\boldsymbol{\theta} - \hat{\boldsymbol{\theta}}_{L^2} \right),$$

where

$$\hat{V}_{L^2} = \frac{\partial^2 \ell_{L^2}(\hat{\boldsymbol{\theta}}_{L^2}; \mathbf{y})}{\partial \boldsymbol{\theta} \partial \boldsymbol{\theta}^T}.$$

(d) As $n \rightarrow \infty$,

$$\sqrt{n} \left(\hat{\boldsymbol{\theta}}_{L^2} - \boldsymbol{\theta}_{L^2} \right) \xrightarrow{d} \mathcal{N} \left(\mathbf{0}, V^{-1} W_{L^2} V^{-1} \right),$$

where

$$W_{L^2} = 4\sigma^2 n \int_{\mathcal{X}} \frac{\eta(\mathbf{x}, \boldsymbol{\theta}_{L^2})}{\partial \boldsymbol{\theta}} \mathbf{s}(\mathbf{x})^T d\mathbf{x} \int_{\mathcal{X}} \mathbf{s}(\mathbf{x}) \frac{\eta(\mathbf{x}, \boldsymbol{\theta}_{L^2})}{\partial \boldsymbol{\theta}^T} d\mathbf{x}.$$

Proof

(a) The proof closely follows that of Theorem 1 of Tuo and Wu (2015) which considers a random design case. Following the definitions of $\boldsymbol{\theta}_{L^2}$ (in C4) and $\hat{\boldsymbol{\theta}}_{L^2}$ (in L1), it is sufficient to show that $\ell_{L^2}(\boldsymbol{\theta}; \mathbf{y})$ converges to $L_{L^2}(\boldsymbol{\theta})$ uniformly with respect to $\boldsymbol{\theta} \in \Theta$ in probability. Note that

$$\begin{aligned} |\ell_{L^2}(\boldsymbol{\theta}; \mathbf{y}, \mathbf{X}) - L_{L^2}(\boldsymbol{\theta})| &= \left| \|\hat{\mu}(\cdot) - \eta(\cdot, \boldsymbol{\theta})\|_{L^2(\mathcal{X})}^2 - \|\mu(\cdot) - \eta(\cdot, \boldsymbol{\theta})\|_{L^2(\mathcal{X})}^2 \right| \\ &= \left| \langle \hat{\mu}(\cdot) - \mu(\cdot), \hat{\mu}(\cdot) + \mu(\cdot) - 2\eta(\cdot, \boldsymbol{\theta}) \rangle_{L^2(\mathcal{X})} \right| \\ &\leq \|\hat{\mu}(\cdot) - \mu(\cdot)\|_{L^2(\mathcal{X})} \|\hat{\mu}(\cdot) + \mu(\cdot) - 2\eta(\cdot, \boldsymbol{\theta})\|_{L^2(\mathcal{X})} \quad (13) \\ &\leq \|\hat{\mu}(\cdot) - \mu(\cdot)\|_{L^2(\mathcal{X})} [\|\hat{\mu}(\cdot)\|_{L^2(\mathcal{X})} + \|\mu(\cdot)\|_{L^2(\mathcal{X})} + 2\|\eta(\cdot, \boldsymbol{\theta})\|_{L^2(\mathcal{X})}] \quad (14) \end{aligned}$$

where lines (13) and (14) follow from the Cauchy-Schwartz and triangle inequalities, respectively. Conditions L3-L6 ensure that the right hand side of (14) converges to 0 as $n \rightarrow \infty$.

(b) For $u, v = 1, \dots, p$,

$$\begin{aligned} \frac{\partial^2 \ell_{L^2}(\boldsymbol{\theta}_{L^2}; \mathbf{y})}{\partial \theta_u \partial \theta_v} &= 2 \left[\left\langle \frac{\partial \eta(\cdot, \boldsymbol{\theta}_{L^2})}{\partial \theta_u}, \frac{\partial \eta(\cdot, \boldsymbol{\theta}_{L^2})}{\partial \theta_v} \right\rangle_{L^2(\mathcal{X})} - \left\langle \frac{\partial^2 \eta(\cdot, \boldsymbol{\theta}_{L^2})}{\partial \theta_u \partial \theta_v}, \hat{\mu}(\cdot) - \eta(\cdot, \boldsymbol{\theta}_{L^2}) \right\rangle_{L^2(\mathcal{X})} \right] \\ &\xrightarrow{p} 2 \left[\left\langle \frac{\partial \eta(\cdot, \boldsymbol{\theta}_{L^2})}{\partial \theta_u}, \frac{\partial \eta(\cdot, \boldsymbol{\theta}_{L^2})}{\partial \theta_v} \right\rangle_{L^2(\mathcal{X})} - \left\langle \frac{\partial^2 \eta(\cdot, \boldsymbol{\theta}_{L^2})}{\partial \theta_u \partial \theta_v}, \mu(\cdot) - \eta(\cdot, \boldsymbol{\theta}_{L^2}) \right\rangle_{L^2(\mathcal{X})} \right] \\ &= V_{uv}, \end{aligned}$$

where the penultimate line follows from condition L4.

(c) This statement follows from Theorem 6 of Miller (2021) under the following provisions.

- (i) There exist $\hat{\boldsymbol{\theta}}_{L^2} \in E \subset \Theta$ such that $\hat{\boldsymbol{\theta}}_{L^2} \xrightarrow{p} \boldsymbol{\theta}_{L^2} \in E$ and $\partial \ell_{L^2}(\hat{\boldsymbol{\theta}}_{L^2}; \mathbf{y}) / \partial \boldsymbol{\theta} = \mathbf{0}$, where E is open and convex.
- (ii) $\partial^2 \ell_{L^2}(\boldsymbol{\theta}_{L^2}; \mathbf{y}, \mathbf{X}) / \partial \boldsymbol{\theta} \partial \boldsymbol{\theta}^T \xrightarrow{p} V$ where V is positive-definite.
- (iii) For $u, v, z = 1, \dots, p$, $\partial^3 \ell_{L^2}(\boldsymbol{\theta}; \mathbf{y}, \mathbf{X}) / \partial \theta_u \partial \theta_v \partial \theta_z$ are continuous and uniformly bounded.

These provisions are satisfied by conditions C4-C5, L1-L2, and statements (a) and (b).

(d) Condition L1 means

$$\mathbf{0} = \frac{\partial \ell_{L^2}(\hat{\boldsymbol{\theta}}_{L^2}; \mathbf{y})}{\partial \boldsymbol{\theta}}.$$

By applying Taylor's theorem

$$\mathbf{0} = \frac{\partial \ell_{L^2}(\boldsymbol{\theta}_{L^2}; \mathbf{y})}{\partial \boldsymbol{\theta}} + \frac{\partial^2 \ell_{L^2}(\tilde{\boldsymbol{\theta}}_{L^2}; \mathbf{y})}{\partial \boldsymbol{\theta} \partial \boldsymbol{\theta}^T} (\hat{\boldsymbol{\theta}}_{L^2} - \boldsymbol{\theta}_{L^2}), \quad (15)$$

where the u th element of $\tilde{\boldsymbol{\theta}}_{L^2}$ lies between the u th elements of $\hat{\boldsymbol{\theta}}_{L^2}$ and $\boldsymbol{\theta}_{L^2}$, for $u = 1, \dots, p$. By the consistency of $\hat{\boldsymbol{\theta}}_{L^2}$ (for $\boldsymbol{\theta}_{L^2}$; see (a)), and condition L4,

$$\frac{\partial^2 \ell_{L^2}(\tilde{\boldsymbol{\theta}}_{L^2}; \mathbf{y})}{\partial \boldsymbol{\theta} \partial \boldsymbol{\theta}^T} \xrightarrow{p} V. \quad (16)$$

Now

$$\frac{\partial \ell_{L^2}(\boldsymbol{\theta}_{L^2}; \mathbf{y})}{\partial \boldsymbol{\theta}} = -2 \int_{\mathcal{X}} \frac{\partial \eta(\mathbf{x}, \boldsymbol{\theta}_{L^2})}{\partial \boldsymbol{\theta}} (\hat{\mu}(\mathbf{x}) - \eta(\mathbf{x}, \boldsymbol{\theta}_{L^2})) d\mathbf{x}.$$

Assuming conditions C1 and L7, and applying Theorem 7 of Georgiev (1988) means that $\hat{\mu}(\mathbf{x})$ converges in distribution to a normal distribution. Therefore $\partial \ell_{L^2}(\boldsymbol{\theta}_{L^2}; \mathbf{y}) / \partial \boldsymbol{\theta}$ converges in distribution to a multivariate normal distribution with mean

$$\begin{aligned} \mathbb{E}_{\mathbf{y}} \left[\frac{\partial \ell_{L^2}(\boldsymbol{\theta}_{L^2}; \mathbf{y})}{\partial \boldsymbol{\theta}} \right] &= -2 \int_{\mathcal{X}} \frac{\partial \eta(\mathbf{x}, \boldsymbol{\theta}_{L^2})}{\partial \boldsymbol{\theta}} (\mathbb{E}_{\mathbf{y}} [\hat{\mu}(\mathbf{x})] - \eta(\mathbf{x}, \boldsymbol{\theta}_{L^2})) d\mathbf{x} \\ &\rightarrow \frac{\partial L_{L^2}(\boldsymbol{\theta}_{L^2})}{\partial \boldsymbol{\theta}} = \mathbf{0}, \end{aligned}$$

as $n \rightarrow \infty$, by conditions C4; and L4, and variance $n^{-1}W_{L^2}$, i.e.

$$\frac{\partial \ell_{L^2}(\boldsymbol{\theta}_{L^2}; \mathbf{y})}{\partial \boldsymbol{\theta}} \xrightarrow{d} N(\mathbf{0}, n^{-1}W_{L^2}). \quad (17)$$

Combining (15), (16) and (17) gives the required result. ■

3.3 Properties of frequentist OLS calibration

In this section, we establish properties of frequentist OLS calibration in a similar fashion to those established for L^2 calibration in Section 3.2. We state the required conditions for OLS calibration.

O1 $\hat{\boldsymbol{\theta}}_{OLS} \in E$ (where E is defined in C4) and are unique.

O2 The errors e_1, \dots, e_n are uniformly sub-Gaussian, i.e. there exists C and σ_0^2 such that

$$\max_{i=1, \dots, n} C \{ \mathbb{E}_{e_i} [\exp(e_i^2/C)] - 1 \} \leq \sigma_0^2.$$

O3 $\ell_{OLS}(\boldsymbol{\theta}; \mathbf{y})$ has continuous and uniformly bounded third derivatives (with respect to $\boldsymbol{\theta}$).

O4 (a) There exists $c_0 > 0$ such that

$$\sum_{i=1}^n (\eta(\mathbf{x}_i, \boldsymbol{\theta}_1) - \eta(\mathbf{x}_i, \boldsymbol{\theta}_2))^2 \leq c_0 (\boldsymbol{\theta}_1 - \boldsymbol{\theta}_2)^T (\boldsymbol{\theta}_1 - \boldsymbol{\theta}_2),$$

for all $\boldsymbol{\theta}_1, \boldsymbol{\theta}_2 \in \Theta$.

(b) For $u, v = 1, \dots, p$, $\sup_{\mathbf{x} \in \mathcal{X}} |\partial \eta(\mathbf{x}, \boldsymbol{\theta}) / \partial \theta_u|$ and $\sup_{\mathbf{x} \in \mathcal{X}} |\partial^2 \eta(\mathbf{x}, \boldsymbol{\theta}) / \partial \theta_u \partial \theta_v|$ are uniformly bounded for $\boldsymbol{\theta} \in B_\epsilon(\boldsymbol{\theta}_{L^2})$.

O5 The design points $\mathbf{x}_1, \dots, \mathbf{x}_n$ are chosen such that

(a) $\sup_{\boldsymbol{\theta} \in \Theta} \left| \frac{1}{n} \sum_{i=1}^n (\mu(\mathbf{x}_i) - \eta(\mathbf{x}_i, \boldsymbol{\theta}))^2 - \int_{\mathcal{X}} (\mu(\mathbf{x}) - \eta(\mathbf{x}, \boldsymbol{\theta}))^2 d\mathbf{x} \right| = O(1)$.

(b) For $u, v = 1, \dots, p$,

$$E \left[\frac{\partial^2 \ell_{OLS}(\boldsymbol{\theta}_{L^2}; \mathbf{y})}{\partial \theta_u \partial \theta_v} \right] - V_{uv} = O(1).$$

(c) $\sqrt{E \left[\frac{\partial \ell_{OLS}(\boldsymbol{\theta}_{L^2}; \mathbf{y})}{\partial \boldsymbol{\theta}^T} \right] E \left[\frac{\partial \ell_{OLS}(\boldsymbol{\theta}_{L^2}; \mathbf{y})}{\partial \boldsymbol{\theta}} \right]}} = O(n^{-1/2})$.

O6 There exists an $M < \infty$ such that $|\mu(\mathbf{x}) - \eta(\mathbf{x}, \boldsymbol{\theta}_{L^2})| < M$ for all $\mathbf{x} \in \mathcal{X}$.

O7 The design points $\mathbf{x}_1, \dots, \mathbf{x}_n$ are chosen such that there exists a $t > 0$ with

$$\frac{\sum_{i=1}^n E \left[\left| \frac{\partial \eta(\mathbf{x}_i, \boldsymbol{\theta}_{L^2})}{\partial \theta_j} e_i \right|^{2+t} \right]}{\left[\sum_{i=1}^n \left(\frac{\partial \eta(\mathbf{x}_i, \boldsymbol{\theta}_{L^2})}{\partial \theta_j} \right)^2 \right]^{2+t}} \rightarrow 0$$

as $n \rightarrow \infty$, for $j = 1, \dots, p$.

Lemma 2 (Frequentist OLS calibration)

Under conditions C1-C6 and O1-O6, the following statements are true.

(a) $\hat{\boldsymbol{\theta}}_{OLS} \xrightarrow{p} \boldsymbol{\theta}_{L^2}$ as $n \rightarrow \infty$.

(b) $\frac{\partial^2 \ell_{OLS}(\boldsymbol{\theta}_{L^2}; \mathbf{y})}{\partial \boldsymbol{\theta} \partial \boldsymbol{\theta}^T} \xrightarrow{p} V$ as $n \rightarrow \infty$.

(c) The OLS loss can be written

$$\ell_{OLS}(\boldsymbol{\theta}; \mathbf{y}) = \ell_{OLS}(\hat{\boldsymbol{\theta}}_{OLS}; \mathbf{y}) + \frac{1}{2} (\boldsymbol{\theta} - \hat{\boldsymbol{\theta}}_{OLS})^T \hat{V}_{OLS} (\boldsymbol{\theta} - \hat{\boldsymbol{\theta}}_{OLS}) + r_n (\boldsymbol{\theta} - \hat{\boldsymbol{\theta}}_{OLS}),$$

where

$$\hat{V}_{OLS} = \frac{\partial^2 \ell_{OLS}(\hat{\boldsymbol{\theta}}_{OLS}; \mathbf{y})}{\partial \boldsymbol{\theta} \partial \boldsymbol{\theta}^T}.$$

(d) As $n \rightarrow \infty$,

$$\sqrt{n} (\hat{\boldsymbol{\theta}}_{OLS} - \boldsymbol{\theta}_{L^2}) \xrightarrow{d} N(\mathbf{0}, V^{-1} W_{OLS} V^{-1}),$$

where

$$W_{OLS} = \frac{4\sigma^2}{n} \sum_{i=1}^n \frac{\eta(\mathbf{x}_i, \boldsymbol{\theta}_{L^2})}{\partial \boldsymbol{\theta}} \frac{\eta(\mathbf{x}_i, \boldsymbol{\theta}_{L^2})}{\partial \boldsymbol{\theta}^T}.$$

Proof

- (a) Following the definitions of $\boldsymbol{\theta}_{L^2}$ (in C4) and $\hat{\boldsymbol{\theta}}_{OLS}$ (in O1), it is sufficient to show that $\ell_{OLS}(\boldsymbol{\theta}; \mathbf{y})$ converges to $L_{L^2}(\boldsymbol{\theta})$ uniformly with respect to $\boldsymbol{\theta} \in \Theta$ in probability. Under conditions C1-C5 and O1-O6, Wong et al. (2017, Lemma 1 proof) showed that $\ell_{OLS}(\boldsymbol{\theta}; \mathbf{y})$ converges to $L_{L^2}(\boldsymbol{\theta}) + \sigma^2$ uniformly with respect to $\boldsymbol{\theta} \in \Theta$ in probability.
- (b) See Wong et al. (2017, Theorem 1 proof), which requires conditions C1-C5 and O1-O6.
- (c) This statement follows from Theorem 6 of Miller (2021) under the following provisions.

- (i) There exist $\hat{\boldsymbol{\theta}}_{OLS} \in E \subset \mathbb{R}^p$ such that $\hat{\boldsymbol{\theta}}_{OLS} \xrightarrow{p} \boldsymbol{\theta}_{L^2} \in E$ and $\partial \ell_{OLS}(\hat{\boldsymbol{\theta}}_{L^2}; \mathbf{y}) / \partial \boldsymbol{\theta} = \mathbf{0}$, where E is open and convex.
- (ii) $\partial^2 \ell_{OLS}(\boldsymbol{\theta}_{L^2}; \mathbf{y}) / \partial \boldsymbol{\theta} \partial \boldsymbol{\theta}^T \xrightarrow{p} V$ where V is positive-definite.
- (iii) For $u, v, z = 1, \dots, p$, $\partial^3 \ell_{OLS}(\boldsymbol{\theta}; \mathbf{y}) / \partial \theta_u \partial \theta_v \partial \theta_z$ are continuous and uniformly bounded.

These provisions are satisfied by conditions C4-C5, O1-O3, and statements (a) and (b).

- (d) Condition O1 implies

$$\mathbf{0} = \frac{\partial \ell_{OLS}(\hat{\boldsymbol{\theta}}_{OLS}; \mathbf{y})}{\partial \boldsymbol{\theta}}.$$

Applying Taylor's theorem

$$\mathbf{0} = \frac{\partial \ell_{OLS}(\boldsymbol{\theta}_{L^2}; \mathbf{y})}{\partial \boldsymbol{\theta}} + \frac{\partial^2 \ell_{OLS}(\bar{\boldsymbol{\theta}}_{L^2}; \mathbf{y})}{\partial \boldsymbol{\theta} \partial \boldsymbol{\theta}^T} (\hat{\boldsymbol{\theta}}_{OLS} - \boldsymbol{\theta}_{L^2}) \quad (18)$$

where the u th element of $\bar{\boldsymbol{\theta}}_{L^2}$ lies between the u th elements of $\hat{\boldsymbol{\theta}}_{OLS}$ and $\boldsymbol{\theta}_{L^2}$, for $u = 1, \dots, p$. By the consistency of $\hat{\boldsymbol{\theta}}_{OLS}$ (for $\boldsymbol{\theta}_{L^2}$; see statement (a)) and that $\partial^2 \ell_{OLS}(\boldsymbol{\theta}_{L^2}; \mathbf{y}) / \partial \boldsymbol{\theta} \partial \boldsymbol{\theta}^T \rightarrow V$ (see statement (b)), we have

$$\frac{\partial^2 \ell_{OLS}(\bar{\boldsymbol{\theta}}_{L^2}; \mathbf{y})}{\partial \boldsymbol{\theta} \partial \boldsymbol{\theta}^T} \xrightarrow{p} V, \quad (19)$$

as $n \rightarrow \infty$. Now

$$\begin{aligned} \frac{\partial \ell_{OLS}(\boldsymbol{\theta}_{L^2}; \mathbf{y})}{\partial \boldsymbol{\theta}} &= -\frac{2}{n} \sum_{i=1}^n \frac{\partial \eta(\mathbf{x}_i, \boldsymbol{\theta}_{L^2})}{\partial \boldsymbol{\theta}} (y_i - \eta(\mathbf{x}_i, \boldsymbol{\theta}_{L^2})) \\ &= -\frac{2}{n} \sum_{i=1}^n \frac{\partial \eta(\mathbf{x}_i, \boldsymbol{\theta}_{L^2})}{\partial \boldsymbol{\theta}} (\mu(\mathbf{x}_i) - \eta(\mathbf{x}_i, \boldsymbol{\theta}_{L^2})) \\ &\quad - \frac{2}{n} \sum_{i=1}^n \frac{\partial \eta(\mathbf{x}_i, \boldsymbol{\theta}_{L^2})}{\partial \boldsymbol{\theta}} (e_i - \eta(\mathbf{x}_i, \boldsymbol{\theta}_{L^2})), \\ &= Q_1 + Q_2. \end{aligned}$$

By conditions C1 and O7, and Lyapunov's theorem (e.g. Billingsley, 1995, page 362), Q_2 converges in distribution to a normal distribution. Then $\partial \ell_{OLS}(\boldsymbol{\theta}_{L^2}; \mathbf{y}) / \partial \boldsymbol{\theta}$ has a multivariate normal distribution with mean

$$E \left[\frac{\partial \ell_{OLS}(\boldsymbol{\theta}_{L^2}; \mathbf{y})}{\partial \boldsymbol{\theta}} \right] = Q_1 = -\frac{2}{n} \sum_{i=1}^n \frac{\partial \eta(\mathbf{x}_i, \boldsymbol{\theta}_{L^2})}{\partial \boldsymbol{\theta}} (\mu(\mathbf{x}_i) - \eta(\mathbf{x}_i, \boldsymbol{\theta}_{L^2})) \rightarrow 0$$

as $n \rightarrow \infty$, by condition O5; and variance $n^{-1} W_{OLS}$. Hence,

$$\frac{\partial \ell_{OLS}(\boldsymbol{\theta}_{L^2}; \mathbf{y})}{\partial \boldsymbol{\theta}} \xrightarrow{d} N(\mathbf{0}, n^{-1} W_{OLS}). \quad (20)$$

Combining (18), (19) and (20) gives the required result. ■

3.4 Automatic scaling

3.4.1 Magnitude scaling

Let $\ell_M(\boldsymbol{\theta}; \mathbf{y})$ denote the loss function where M can be either L^2 or OLS. Correspondingly, let $\hat{\boldsymbol{\theta}}_M$ be the the values of $\boldsymbol{\theta} \in \Theta$ that minimise $\ell_M(\boldsymbol{\theta}; \mathbf{y})$, as defined in conditions L1 (for $M = L^2$) and O1 (for $M = \text{OLS}$). First consider *magnitude scaling* with loss function, generalised likelihood and generalised posterior given by

$$\begin{aligned}\ell_M^{(mag)}(\boldsymbol{\theta}; \mathbf{y}) &= \gamma \ell_M(\boldsymbol{\theta}; \mathbf{y}), \\ \pi_{G:M}^{(mag)}(\mathbf{y}|\boldsymbol{\theta}) &= \exp[-\gamma \ell_M(\boldsymbol{\theta}; \mathbf{y})] \\ \pi_{G:M}^{(mag)}(\boldsymbol{\theta}|\mathbf{y}) &= \exp[-\gamma \ell_M(\boldsymbol{\theta}; \mathbf{y})] \pi(\boldsymbol{\theta}),\end{aligned}$$

respectively, where $\gamma > 0$ does not depend on $\boldsymbol{\theta}$ and $\pi(\cdot)$ is the density of the prior distribution for $\boldsymbol{\theta}_{L^2}$. Analogous to the likelihood ratio statistic in (12), define

$$\begin{aligned}\Lambda_M^{(mag)}(\boldsymbol{\theta}_{L^2}; \mathbf{y}) &= 2n \left[\ell_M^{(mag)}(\boldsymbol{\theta}_{L^2}; \mathbf{y}) - \ell_M^{(mag)}(\hat{\boldsymbol{\theta}}_M; \mathbf{y}) \right] \\ &= 2n\gamma \left[\ell_M(\boldsymbol{\theta}_{L^2}; \mathbf{y}) - \ell_M(\hat{\boldsymbol{\theta}}_M; \mathbf{y}) \right].\end{aligned}$$

The goal is to determine a value $\gamma_M^* > 0$ for γ to ensure the asymptotic expectation of $\Lambda_M^{(mag)}(\boldsymbol{\theta}_{L^2}; \mathbf{y})$ is the same as p : the asymptotic expectation of the likelihood ratio statistic $\Lambda_0(\boldsymbol{\theta}_0, \mathbf{y})$. By statement (c) of Lemma 1 (for $M = L^2$) or Lemma 2 (for $M = \text{OLS}$),

$$\Lambda_M^{(mag)}(\boldsymbol{\theta}_{L^2}; \mathbf{y}) = n\gamma \left(\boldsymbol{\theta}_{L^2} - \hat{\boldsymbol{\theta}}_M \right)^T \hat{V}_M \left(\boldsymbol{\theta}_{L^2} - \hat{\boldsymbol{\theta}}_M \right) + 2n\gamma r_n \left(\boldsymbol{\theta}_{L^2} - \hat{\boldsymbol{\theta}}_M \right).$$

Then, by statements (a), (b) and (d) of Lemma 1 (for $M = L^2$) or Lemma 2 (for $M = \text{OLS}$),

$$\mathbb{E} \left[\Lambda_M^{(mag)}(\boldsymbol{\theta}_{L^2}; \mathbf{y}) \right] \rightarrow \gamma \text{tr} (V^{-1} W_M),$$

as $n \rightarrow \infty$, since $\hat{V}_M \xrightarrow{p} V$. Equating the asymptotic expectation of $\Lambda_M^{(mag)}(\boldsymbol{\theta}_{L^2}; \mathbf{y})$ to p yields

$$\gamma_M^* = \frac{p}{\text{tr} (V^{-1} W_M)}.$$

3.4.2 Curvature scaling

Curvature scaling has loss function, generalised likelihood and generalised posterior given by

$$\begin{aligned}\ell_M^{(cur)}(\boldsymbol{\theta}; \mathbf{y}) &= \gamma_M^* \ell_M \left(\hat{\boldsymbol{\theta}}_M + \Gamma \left(\boldsymbol{\theta} - \hat{\boldsymbol{\theta}}_M \right); \mathbf{y} \right), \\ \pi_{G:M}^{(cur)}(\mathbf{y}|\boldsymbol{\theta}) &= \exp \left[-\gamma_M^* \ell_M \left(\hat{\boldsymbol{\theta}}_M + \Gamma \left(\boldsymbol{\theta} - \hat{\boldsymbol{\theta}}_M \right); \mathbf{y} \right) \right] \\ \pi_{G:M}^{(cur)}(\boldsymbol{\theta}|\mathbf{y}) &= \exp \left[-\gamma_M^* \ell_M \left(\hat{\boldsymbol{\theta}}_M + \Gamma \left(\boldsymbol{\theta} - \hat{\boldsymbol{\theta}}_M \right); \mathbf{y} \right) \right] \pi(\boldsymbol{\theta}),\end{aligned}\tag{21}$$

where $\Gamma \in G$ is a $p \times p$ matrix, independent of $\boldsymbol{\theta}$, and G is a subset of the space of $p \times p$ positive-definite matrices. The definition of the curvature scaling loss function in (21) is different to that proposed by Ribatet et al. (2012) in that we include the factor γ_M^* . However, as we show below, inclusion of γ_M^* means

that magnitude and curvature scaling coincide for $p = 1$ calibration parameters. If $\hat{\boldsymbol{\theta}}_M + \Gamma(\boldsymbol{\theta} - \hat{\boldsymbol{\theta}}) \in \Theta$ for all $\boldsymbol{\theta} \in \Theta$ and $\Gamma \in G$, then $\hat{\boldsymbol{\theta}}_M = \arg \min_{\boldsymbol{\theta} \in \Theta} \ell_M^{(cur)}(\boldsymbol{\theta}; \mathbf{y})$. Define

$$\Lambda_M^{(cur)}(\boldsymbol{\theta}_{L^2}; \mathbf{y}) = 2n \left[\ell_M^{(cur)}(\boldsymbol{\theta}_{L^2}; \mathbf{y}) - \ell_M^{(cur)}(\hat{\boldsymbol{\theta}}_M; \mathbf{y}) \right].$$

By statement (c) of Lemma 1 ($M = L^2$) or Lemma 2 ($M = \text{OLS}$),

$$\begin{aligned} \Lambda_M^{(cur)}(\boldsymbol{\theta}_{L^2}; \mathbf{y}) &= n\gamma_M^* (\boldsymbol{\theta}_{L^2} - \hat{\boldsymbol{\theta}}_M)^T \Gamma^T \frac{\partial^2 \ell_M(\hat{\boldsymbol{\theta}}_M + \Gamma(\boldsymbol{\theta}_{L^2} - \hat{\boldsymbol{\theta}}_M); \mathbf{y})}{\partial \boldsymbol{\theta} \partial \boldsymbol{\theta}^T} \Gamma (\boldsymbol{\theta}_{L^2} - \hat{\boldsymbol{\theta}}_M) \\ &\quad + 2n\gamma_M^* r_n(\boldsymbol{\theta}_{L^2} - \hat{\boldsymbol{\theta}}_M). \end{aligned}$$

By statements (a) and (b) of Lemma 1 ($M = L^2$) or Lemma 2 ($M = \text{OLS}$),

$$\frac{\partial^2 \ell_M(\hat{\boldsymbol{\theta}}_M + \Gamma(\boldsymbol{\theta}_{L^2} - \hat{\boldsymbol{\theta}}_M); \mathbf{y})}{\partial \boldsymbol{\theta} \partial \boldsymbol{\theta}^T} \xrightarrow{p} V. \quad (22)$$

Curvature scaling involves specifying a $\Gamma_M^* \in G$ for Γ such that $\Lambda_M^{(cur)}(\boldsymbol{\theta}_{L^2}; \mathbf{y})$ converges in distribution to χ_p^2 . By statement (d) of Lemma 1 ($M = L^2$) or Lemma 2 ($M = \text{OLS}$), this can be achieved by specifying Γ_M^* such that

$$\gamma_M^* \Gamma_M^{*T} V \Gamma_M^* = V W_M^{-1} V, \quad (23)$$

i.e. the right-hand side of (23) is the inverse of the variance matrix of $\hat{\boldsymbol{\theta}}_M$. A Γ_M^* satisfying (23) is not unique but, following Ribatet et al. (2012), we let

$$\Gamma_M^* = Q_M^{-1} P_M,$$

where P_M and Q_M are $p \times p$ matrices satisfying $P_M^T P_M = V W_M^{-1} V$ and $Q_M^T Q_M = \gamma_M^* V$.

3.4.3 Discussion

Note that γ_M^* and Γ_M^* depend on the unknown σ^2 , $\mu(\mathbf{x})$ and $\boldsymbol{\theta}_{L^2}$. Instead, we use consistent estimators

$$\hat{\gamma}_M^* = \frac{p}{\text{tr}(\hat{V}_M^{-1} \hat{W}_M)}, \quad \text{and} \quad \hat{\Gamma}_M^* = \hat{Q}_M^{-1} \hat{P}_M$$

where $\hat{P}_M^T \hat{P}_M = \hat{V}_M \hat{W}_M^{-1} \hat{V}_M$ and $\hat{Q}_M^T \hat{Q}_M = \hat{\gamma}_M^* \hat{V}_M$ with

$$\begin{aligned} \hat{W}_{L^2} &= 4\hat{\sigma}^2 n \int_{\mathcal{X}} \frac{\partial \eta(\mathbf{x}, \hat{\boldsymbol{\theta}}_{L^2})}{\partial \boldsymbol{\theta}} \mathbf{s}(\mathbf{x})^T d\mathbf{x} \int_{\mathcal{X}} \mathbf{s}(\mathbf{x}) \frac{\partial \eta(\mathbf{x}, \hat{\boldsymbol{\theta}}_{L^2})}{\partial \boldsymbol{\theta}} d\mathbf{x} \\ \hat{W}_{OLS} &= \frac{4\hat{\sigma}^2}{n} \sum_{i=1}^n \frac{\partial \eta(\mathbf{x}_i, \hat{\boldsymbol{\theta}}_{OLS})}{\partial \boldsymbol{\theta}} \frac{\partial \eta(\mathbf{x}_i, \hat{\boldsymbol{\theta}}_{OLS})}{\partial \boldsymbol{\theta}^T} \end{aligned}$$

and

$$\hat{\sigma}^2 = \frac{\sum_{i=1}^n (y_i - \hat{\mu}(\mathbf{x}_i))^2}{n - \text{tr}(S)},$$

a consistent estimator of σ^2 (under condition L4).²

In the case when $p = 1$

$$\hat{\Gamma}_M^* = \frac{\sqrt{\hat{V}_M \hat{W}_M^{-1} \hat{V}_M}}{\sqrt{\hat{\gamma}_M^* \hat{V}_M}} = \frac{\sqrt{\hat{V}_M \hat{W}_M^{-1}}}{\sqrt{\hat{\gamma}_M^*}} = 1,$$

resulting in magnitude and curvature scaling coinciding.

To illustrate the automatic scaling methods, consider the illustrative example in Section 2.4. For the set of responses shown in Figure 1(a), we estimate $\hat{\gamma}_{L^2}^* = 17.80$ and $\hat{\gamma}_{OLS}^* = 8.899$. Figure 1(b) shows the generalised posterior distribution under L^2 and OLS loss functions and these two values, respectively. The true θ_{L^2} now features in a region of relative high posterior density for both of the distributions. The respective posterior means are 3.585 and 3.363.

Woody et al. (2019) considered a similar idea for scaling the L^2 loss under magnitude scaling. They specify $\gamma_{L^2}^*$ such that coverage of probability intervals from the general posterior distribution match the confidence intervals from the frequentist analysis. The value of $\gamma_{L^2}^*$ is estimated via a bootstrap procedure.

4 Asymptotic behaviour of the generalised posterior distribution

In this section we consider theoretic properties of the generalised posterior distribution for $\boldsymbol{\theta}$ under L^2 and OLS loss functions, and the magnitude and curvature scaling described in Section 3.4.

First, let $\ell_M^S(\boldsymbol{\theta}; \mathbf{y})$ denote the scaled loss where $M \in \{L^2, \text{OLS}\}$ and $S \in \{\text{(mag)}, \text{(cur)}\}$. The corresponding generalised posterior distribution is

$$\pi_{G:M}^S(\boldsymbol{\theta}|\mathbf{y}) \propto \exp(-n\ell_M^S(\boldsymbol{\theta}; \mathbf{y})) \pi(\boldsymbol{\theta}).$$

Similarly, the expected scaled loss is denoted

$$L_M^S(\boldsymbol{\theta}) = \mathbb{E}[\ell_M^S(\boldsymbol{\theta}; \mathbf{y})].$$

The target parameters are

$$\boldsymbol{\theta}_M^S = \arg \min_{\boldsymbol{\theta} \in \Theta} L_M^S(\boldsymbol{\theta}).$$

In general, $\boldsymbol{\theta}_M^S \neq \boldsymbol{\theta}_{L^2}$ for finite n . However, we shortly show that $\boldsymbol{\theta}_M^S \rightarrow \boldsymbol{\theta}_{L^2}$, as $n \rightarrow \infty$, as well as other asymptotic properties of the generalised posterior, $\pi_{G:M}^S(\boldsymbol{\theta}|\mathbf{y})$, namely concentration and a limiting distribution.

We need some extra conditions as follows.

E1 The prior density $\pi(\boldsymbol{\theta})$ is continuous and positive at $\boldsymbol{\theta} = \boldsymbol{\theta}_{L^2}$.

E2 $\boldsymbol{\theta}_M^S \in E$ (where E is defined in C4) and are unique.

E3 As $n \rightarrow \infty$

- (a) $\hat{\gamma}_M^* \xrightarrow{p} \gamma_M^*$;
- (b) $\hat{\Gamma}_M^* \xrightarrow{p} \Gamma_M^*$.

E4 $\hat{\boldsymbol{\theta}}_M + \Gamma(\boldsymbol{\theta} - \hat{\boldsymbol{\theta}}_M) \in \Theta$ and $\boldsymbol{\theta}_{L^2} + \Gamma(\boldsymbol{\theta} - \boldsymbol{\theta}_{L^2}) \in \Theta$ for all $\boldsymbol{\theta} \in \Theta$ and $\Gamma \in G$.

E5 $L_M^S(\boldsymbol{\theta})$ is bounded for $\boldsymbol{\theta} \in E$, and has continuous and uniformly bounded third derivatives.

Theorem 1

Under one set of the following conditions

- C1-C6, L1-L7 (for L^2 calibration);
- C1-C6, O1-O7 (for OLS calibration);

and conditions E1 - E5, the following statements are true.

- (a) (Convergence of target parameter values). $\boldsymbol{\theta}_M^S \rightarrow \boldsymbol{\theta}_{L^2}$, as $n \rightarrow \infty$.
- (b) (Concentration of generalised posterior distribution). $\int_{B_\epsilon(\boldsymbol{\theta}_{L^2})} \pi_{G:M}^S(\boldsymbol{\theta}|\mathbf{y}) d\boldsymbol{\theta} \xrightarrow{p} 1$, as $n \rightarrow \infty$, for all $\epsilon > 0$.
- (c) (Limiting distribution). Let $Q_n = \sqrt{n}(\boldsymbol{\theta} - \hat{\boldsymbol{\theta}}_M)$, where the pdf of $\boldsymbol{\theta}$ is $\pi_{G:M}^S(\boldsymbol{\theta}|\mathbf{y})$. Then the distribution of Q_n converges to

$$N(\mathbf{0}, \Sigma_S^{-1}),$$

in total variation, where

$$\Sigma_S = \begin{cases} \gamma_M^* V & \text{if } S = (mag); \\ \gamma_M^* \Gamma_M^{*T} V \Gamma_M^* = V W_M^{-1} V & \text{if } S = (cur). \end{cases}$$

Proof

Statement (a)

By conditions C4, E2 and E4, it is sufficient to show that $L_M^S(\boldsymbol{\theta})$ converges uniformly to

$$\bar{L}_M^S(\boldsymbol{\theta}) = \begin{cases} c + \gamma_M^* L_{L^2}(\boldsymbol{\theta}) & \text{if } S = (mag); \\ c + \gamma_M^* L_{L^2}(\boldsymbol{\theta}_{L^2} + \Gamma_M^*(\boldsymbol{\theta} - \boldsymbol{\theta}_{L^2})) & \text{if } S = (cur); \end{cases}$$

with $\boldsymbol{\theta}_{L^2} = \arg \min_{\boldsymbol{\theta} \in \Theta} L_{L^2}(\boldsymbol{\theta})$ and c a constant. However, under Theorem 7 of Miller (2021), and assumption of condition E5, it is sufficient to show that $L_M^S(\boldsymbol{\theta})$ converges pointwise to $\bar{L}_M^S(\boldsymbol{\theta})$.

If $M = L^2$, the proof of statement (a) in Lemma 1 shows that $\ell_{L^2}(\boldsymbol{\theta}; \mathbf{y})$ converges uniformly (with respect to $\boldsymbol{\theta}$) to $L_{L^2}(\boldsymbol{\theta})$ in probability. By the continuous mapping theorem, the consistency of $\hat{\boldsymbol{\theta}}_M$ and condition E3, $\ell_M^{L^2}(\boldsymbol{\theta}) \xrightarrow{p} \bar{L}_{L^2}^S(\boldsymbol{\theta})$. It follows that $L_{L^2}^S(\boldsymbol{\theta}) = E_{\mathbf{y}}[\ell_{L^2}^S(\boldsymbol{\theta})] \rightarrow \bar{L}_{L^2}^S(\boldsymbol{\theta})$, with $c = 0$, as required.

Now if $M = OLS$, the proof of statement (a) in Lemma 2 shows that $\ell_{OLS}(\boldsymbol{\theta}; \mathbf{y})$ converges uniformly (with respect to $\boldsymbol{\theta}$) to $\sigma^2 + L_{L^2}(\boldsymbol{\theta})$ in probability. Similar to above, it follows that $L_{OLS}^S(\boldsymbol{\theta}) = E_{\mathbf{y}}[\ell_{OLS}^S(\boldsymbol{\theta})] \rightarrow \bar{L}_{OLS}^S(\boldsymbol{\theta})$, with $c = \sigma^2$, as required.

Statements (b) and (c)

The proof is provided by Theorem 4 of Miller (2021) if the following provisions are true.

- (i) Condition E1.
- (ii) The Taylor series expansion in statement (c) of Lemmas 1 (for $M = L^2$) or Lemma 2 (for $M = OLS$).
- (iii) $\liminf_n \inf_{\boldsymbol{\theta} \in B_\epsilon(\hat{\boldsymbol{\theta}}_M)^c} [\ell_M(\boldsymbol{\theta}; \mathbf{y}) - \ell_M(\hat{\boldsymbol{\theta}}_M; \mathbf{y})] > 0$ for all $\epsilon > 0$. This is ensured by conditions L1 (for $M = L^2$) or O1 (for $M = OLS$). ■

Consider the result given by part (c) of Theorem 1. Under loss function M and magnitude scaling, the asymptotic generalised posterior variance of $\boldsymbol{\theta}_{L^2}$ is

$$\text{var}^{(mag)}(\boldsymbol{\theta}_{L^2}|\mathbf{y}, M) = \frac{1}{n\gamma_M^*} V^{-1} = \frac{\text{tr}(V^{-1}W_M) V^{-1}}{np}.$$

The determinant of $\text{var}^{(mag)}(\boldsymbol{\theta}_{L^2}|\mathbf{y}, M)$ (a scalar measure of variability for a multivariate distribution; Wilkes 1932) is then

$$\begin{aligned} |\text{var}^{(mag)}(\boldsymbol{\theta}_{L^2}|\mathbf{y}, M)| &= \frac{\text{tr}(V^{-1}W_M)^p |V|^{-1}}{n^p p^p} \\ &\geq \frac{|V^{-1}W_M| |V|^{-1}}{n^p} \\ &= \left| \frac{1}{n} V^{-1} W_M V^{-1} \right| \end{aligned}$$

The inequality above follows from the fact that the arithmetic mean of the eigenvalues of $V^{-1}W_M$ is greater or equal to the geometric mean. Therefore, under magnitude scaling, the asymptotic variability (as measured by the determinant) of the generalised posterior is greater than that of the frequentist estimator $\hat{\boldsymbol{\theta}}_M$. By contrast, under curvature scaling, the asymptotic generalised posterior variance is equation that of $\hat{\boldsymbol{\theta}}_M$. We compare the practical difference between magnitude and curvature scaling by way of simulation studies and real applications in Section 6.

5 Practical implications

5.1 Comparison of OLS calibration and traditional Bayesian inference under normal errors

In this section, we consider the apparent similarity between general Bayesian OLS calibration and traditional Bayesian inference under the assumption that the errors e_1, \dots, e_n are an independent and identically distributed sample from a normal distribution with mean zero and constant variance (denoted here by τ^2).

The likelihood is given by

$$\pi(\mathbf{y}|\boldsymbol{\theta}, \tau^2) = (2\pi)^{-\frac{n}{2}} (\tau^2)^{-\frac{n}{2}} \exp \left[-\frac{n\ell_{OLS}(\boldsymbol{\theta}; \mathbf{y})}{2\tau^2} \right].$$

Following Section 2.3, the corresponding expected self-information loss is

$$L_{SI}(\boldsymbol{\theta}, \tau^2) = \mathbb{E}_{\mathbf{y}} \left[-\frac{1}{n} \log \pi(\mathbf{y}|\boldsymbol{\theta}, \tau^2) \right] = \frac{1}{2} \log(2\pi) + \frac{1}{2} \log \tau^2 + \frac{1}{2\tau^2} \mathbb{E}_{\mathbf{y}} [\ell_{OLS}(\boldsymbol{\theta}; \mathbf{y})].$$

The target values $\boldsymbol{\theta}_{SI}$ and τ_{SI}^2 are given by minimising $L_{SI}(\boldsymbol{\theta}, \tau^2)$ with respect to $\boldsymbol{\theta}$ and τ^2 .

Assume conditions C1-C6 and O1-O7, then the proof of Lemma 2 in Wong et al. (2017) shows that $\ell_{OLS}(\boldsymbol{\theta}; \mathbf{y})$ converges uniformly (with respect to $\boldsymbol{\theta}$) to $L_{L^2}(\boldsymbol{\theta}) + \sigma^2$ in probability, as $n \rightarrow \infty$. Hence $L_{SI}(\boldsymbol{\theta}, \tau^2)$ converges uniformly to $\frac{1}{2} \log(2\pi) + \frac{1}{2} \log \tau^2 + \frac{1}{2\tau^2} (L_{L^2}(\boldsymbol{\theta}) + \sigma^2)$, and therefore $\boldsymbol{\theta}_{SI} \rightarrow \boldsymbol{\theta}_{L^2}$. This means that the

asymptotic target calibration parameters of traditional Bayesian inference match those of general Bayesian L^2 and OLS calibration.

However, the target value, τ_{SI}^2 , for τ^2 is

$$\tau_{SI}^2 = \mathbb{E}_{\mathbf{y}} [\ell_{OLS}(\boldsymbol{\theta}_{SI}; \mathbf{y})] = \ell_{OLS}(\boldsymbol{\theta}; \boldsymbol{\mu}) + \sigma^2 \rightarrow L_{L^2}(\boldsymbol{\theta}_{L^2}) + \sigma^2,$$

where $\boldsymbol{\mu} = (\mu(\mathbf{x}_1), \dots, \mu(\mathbf{x}_n))^T$. Therefore the target value for τ^2 has $\tau_{SI}^2 \geq \sigma^2$. In the limit, equality occurs if and only if $L_{L^2}(\boldsymbol{\theta}_{L^2}) = 0$, i.e. the mathematical model is exact.

Now consider the conditional posterior distribution of $\boldsymbol{\theta}$ (given τ^2) given by

$$\pi(\boldsymbol{\theta} | \mathbf{y}, \tau^2) \propto \pi(\mathbf{y} | \boldsymbol{\theta}, \tau^2) \pi(\boldsymbol{\theta} | \tau^2).$$

Suppose $\pi(\boldsymbol{\theta} | \tau^2)$ is continuous and positive at $\boldsymbol{\theta} = \boldsymbol{\theta}_{L^2}$. Theorem 4 of Miller (2021) implies a limiting normal distribution applies for the conditional posterior. Let $Q_n = \sqrt{n} (\boldsymbol{\theta} - \hat{\boldsymbol{\theta}}_{OLS})$ where the pdf of $\boldsymbol{\theta}$ is $\pi(\boldsymbol{\theta} | \mathbf{y}, \tau^2)$. Then the distribution of Q_n converges to $N(\mathbf{0}, \Sigma_{SI}^{-1})$, where

$$\Sigma_{SI} = \frac{1}{2\tau^2} V.$$

Therefore, the variance of the conditional posterior of $\boldsymbol{\theta}$ is proportional to τ^2 . Thus if traditional Bayesian inference targets a value, τ_{SI}^2 , of τ^2 greater than σ^2 , then we expect the variance of the conditional posterior of $\boldsymbol{\theta}$ to be inflated. The amount of inflation is controlled by the size of $\ell_{OLS}(\boldsymbol{\theta}; \boldsymbol{\mu})$ relative to σ^2 . We investigate this issue empirically in Section 6.1 using simulation studies, where traditional Bayesian inference is compared to general Bayesian L^2 and OLS calibration.

5.2 Computation

There are several computational issues to address for the practical implementation of general Bayesian calibration. In particular, the evaluation of the L^2 loss and the generalised posterior distribution (under both L^2 and OLS loss functions).

The L^2 loss, given by (3), involves a k -dimensional integral which will typically be analytically intractable. We use multivariate quadrature to approximate this integral, implicitly assuming that the number of input variables, k , is small. Then

$$\hat{\ell}_{L^2}(\boldsymbol{\theta}; \mathbf{y}) = \sum_{v=1}^V w^{(v)} \left(\hat{\mu}(\mathbf{x}^{(v)}) - \eta(\mathbf{x}^{(v)}, \boldsymbol{\theta}) \right)^2,$$

where $\{\mathbf{x}^{(v)}\}_{v=1}^V$ are V quadrature points in $\mathcal{X} = [0, 1]^k$, with weights $\{w^{(v)}\}_{v=1}^V$. In particular, we use the Gauss-Legendre quadrature scheme with 25 points per each of the k dimensions. Then the number of quadrature points is $V = 25^k$.

To evaluate the generalised posterior distribution we use Markov chain Monte Carlo (MCMC) methods. Since the generalised posterior density is known up to a normalising constant, a large suite of MCMC methods are available in the literature to address this problem. For simplicity, we use a random-walk Metropolis-Hastings algorithm (e.g. O'Hagan and Forster, 2004, pages 267 - 269). In particular, the proposal distribution is a multivariate normal distribution with mean $\mathbf{0}$ and variance $\epsilon \hat{\Sigma}_S^{-1}$ where $\epsilon > 0$ and

$$\hat{\Sigma}_S = \begin{cases} \hat{\gamma}_M^* \hat{V}_M & \text{if } S = (\text{mag}); \\ \hat{V}_M \hat{W}_M^{-1} \hat{V}_M & \text{if } S = (\text{cur}), \end{cases}$$

where $M \in \{L^2, \text{OLS}\}$. Thus we specify the proposal variance to be proportional to the variance of the limiting generalised posterior distribution as given by Theorem 1 in Section 4. The constant ϵ is specified, using pilot chains, to ensure the acceptance rate of the algorithm is between 10% and 40% (described as close to optimal by Roberts and Rosenthal 2001).

6 Examples

6.1 Synthetic examples

6.1.1 Introduction

We begin by considering synthetic, but illustrative, examples with which we investigate the performance of different calibration methods.

There are four configurations, each defined by a mathematical model given in Section 6.1.2. In each configuration, the true physical process $\mu(\mathbf{x})$ is known. Correspondingly the true values of $\boldsymbol{\theta}_{L^2}$ can be determined. We generate responses from the true physical process and implement five different calibration approaches as follows.

- general Bayesian calibration under L^2 loss and magnitude and curvature (if $p > 1$) scaling;
- general Bayesian calibration under OLS loss and magnitude and curvature (if $p > 1$) scaling; and
- traditional Bayesian inference under normal errors.

We repeat this process 500 times for a range of different values of n . We then compare the calibration approaches using the mean generalised posterior mean and standard deviation, and the coverage of 95% highest generalised posterior density (HGPD) intervals for the elements of $\boldsymbol{\theta}_{L^2}$. In the case of traditional Bayesian inference, we use the mean posterior mean and standard deviation, and coverage of 95% highest posterior density (HPD) intervals.

6.1.2 Configurations

Each of the four configurations have been considered previously by Plumlee (2017), Wong et al. (2017), Gu and Wang (2018) and Xie and Xu (2021). The setup considered here significantly expands on their treatment by studying long-run performance and a greater range of values of n . For Configurations 2 and 3, there is only $p = 1$ calibration parameter so magnitude and curvature scaling are identical.

Configuration 1. The mathematical model, with $k = 1$ and $p = 2$, is

$$\eta(x, \boldsymbol{\theta}) = 7[\sin(2\pi\theta_1 - \pi)]^2 + 2[(2\pi\theta_2 - \pi)^2 \sin(2\pi x - \pi)],$$

where $\boldsymbol{\theta} = (\theta_1, \theta_2)^T$. The physical process is $\mu(x) = \eta(x, \boldsymbol{\theta}_0)$ with $\boldsymbol{\theta}_0 = (0.2, 0.3)^T$, i.e. the mathematical model is exact. It follows that $\boldsymbol{\theta}_{L^2} = \boldsymbol{\theta}_0$. We simulate n responses via $y_i = \mu(x_i) + e_i$, for $i = 1, \dots, n$, where $e_i \stackrel{\text{iid}}{\sim} N(0, \sigma^2)$, with $\sigma^2 = 0.2^2$, and x_1, \dots, x_n are equally-spaced on \mathcal{X} . We consider $n = 25, 50, \dots, 200$. Xie and Xu (2021) considered $n = 50$ with a random design. The prior distribution for $\boldsymbol{\theta}_{L^2}$ is such that the elements are independent with $\theta_{L^2,1} \sim U(0, 0.25)$ and $\theta_{L^2,2} \sim U(0, 0.5)$.

Configuration 2. The mathematical model, with $k = 1$ and $p = 1$, is

$$\eta(x, \theta) = \sin(5\theta x) + 5x$$

and the physical process is

$$\mu(x) = 5x \cos(15x/2) + 5x.$$

The value of θ minimising $L_{L^2}(\theta)$ can be found numerically as $\theta_{L^2} = 1.8772$. We simulate n responses via $y_i = \mu(x_i) + e_i$, for $i = 1, \dots, n$, where $e_i \stackrel{\text{iid}}{\sim} N(0, \sigma^2)$, with $\sigma^2 = 0.2^2$, and x_1, \dots, x_n are equally-spaced on \mathcal{X} . We consider $n = 30, 60, \dots, 240$. Xie and Xu (2021) and Gu and Wang (2018) considered $n = 30$. The prior distribution for θ_{L^2} is $U(0, 3)$.

Configuration 3. The mathematical model, with $k = 1$ and $p = 1$, true physical process, and corresponding value of θ_{L^2} are given in the illustrative example in Section 2.4. We consider two different designs: (i) x_1, \dots, x_n are equally-spaced on \mathcal{X} ; and (ii) x_1, \dots, x_n are equally-spaced on $\mathcal{X}' = [0, 0.8]$. Xie and Xu (2021) and Plumlee (2017) considered $n = 17$ with data-generation specification (i) and (ii), respectively.

For design specification (ii), the feature that the space on which the inputs x_1, \dots, x_n are selected, \mathcal{X}' , is a subset of \mathcal{X} represents the situation where the controllable variables in an experiment cannot be selected from some regions of \mathcal{X} . If we define an L^2 loss on \mathcal{X}' , i.e.

$$L'_{L^2}(\theta) = \int_{\mathcal{X}'} (\mu(x) - \eta(x, \theta))^2 dx,$$

then its minimiser is

$$\theta'_{L^2} = \arg \min L'_{L^2}(\theta) = 4.0514.$$

By Theorem 1, this is the target parameter for OLS calibration.

Configuration 4.

The mathematical model, with $k = 2$ and $p = 3$, is

$$\eta(\mathbf{x}, \boldsymbol{\theta}) = 7 \sin^2(2\pi\theta_1 - \pi) + 2(2\pi\theta_2 - \pi)^2 \sin(2\pi x_1 - \pi) + 6\theta_3 \left(x_2 - \frac{1}{2} \right),$$

and the physical process is

$$\mu(\mathbf{x}) = \eta(\mathbf{x}, \boldsymbol{\theta}_0) + \cos(2\pi x_1 - \pi) + 2 \left(x_2^2 - x_2 + \frac{1}{6} \right),$$

where $\boldsymbol{\theta}_0 = (0.2, 0.3, 0.8)^T$. The values of $\boldsymbol{\theta}$ that minimise $L_{L^2}(\boldsymbol{\theta})$ are $\boldsymbol{\theta}_{L^2} = \boldsymbol{\theta}_0$. We simulate n responses via $y_i = \mu(\mathbf{x}_i) + e_i$, for $i = 1, \dots, n$, where $e_i \stackrel{\text{iid}}{\sim} N(0, \sigma^2)$ with (following Wong et al. 2017)

$$\sigma^2 = \frac{1}{10} \int_{\mathcal{X}} \left[\mu(\mathbf{x}) - \int_{\mathcal{X}} \mu(\mathbf{x})^2 d\mathbf{x} \right]^2 d\mathbf{x} = 0.7430.$$

The inputs $\mathbf{x}_1, \dots, \mathbf{x}_n$ are the points of a maximum projection Latin hypercube design (Joseph et al., 2015) found using the R package **MaxPro** (Ba and Joseph, 2018). We consider $n = 30, 40, \dots, 100, 150, \dots, 400$. Wong et al. (2017) considered $n = 50$. We assume the following independent prior distributions for the elements of $\boldsymbol{\theta}_{L^2}$

$$\theta_{L^2,1} \sim U[0, 0.25]; \quad \theta_{L^2,2} \sim U[0, 0.5]; \quad \theta_{L^2,3} \sim U[0, 1];$$

following the parameter spaces considered by Wong et al. (2017).

6.1.3 Results

Configuration 1 The results for Configuration 1 are summarised by Figure 2 for θ_1 (left-hand panels) and θ_2 (right-hand). The first and second rows show the mean (over the 500 replications) of the generalised posterior mean and log standard deviation plotted against n . The third rows show the coverage of the 95% H(G)PD intervals plotted against n . In this case, when the mathematical model is exact, all five methods perform similarly except for the smallest value of $n = 50$. Here, traditional Bayesian inference has coverage closer to the nominal 95% than the general Bayesian approaches. Finally, there is negligible difference between magnitude and curvature scaling.

Configuration 2 The results for Configuration 2 are summarised by column (a) of Figure 3. The organisation of the figure rows are identical to those in Figure 2. The posterior mean for general Bayesian calibration under the L^2 loss is closer to the true θ_{L^2} than under the OLS loss. This bias for the OLS loss causes significant under-coverage of the HGPD intervals evident in the last row. As expected, from Section 5.1, since the mathematical model is inexact, the posterior standard deviation under traditional Bayesian calibration is inflated (when compared to the general Bayesian approaches). We can provide some further insight here by stating that $L_{L^2}(\theta_{L^2}) = 2.866$ with $\sigma^2 = 0.2^2 = 0.04$, so the target response variance for traditional Bayesian calibration is $\tau_{SI}^2 = 2.906$. This causes the over-coverage of the HPD intervals for traditional Bayesian calibration.

Configuration 3 The results for Configuration 3 are summarised by columns (b) and (c) of Figure 3, for designs with support $\mathcal{X} = [0, 1]$ and $\mathcal{X}' = [0, 0.8]$, respectively. The organisation of the figure rows are identical to those in Figure 2. The scale of the y -axis for the first row of Figure 3 (b) and (c) is the same to aid comparison.

When the support for the design is $\mathcal{X} = [0, 1]$, the results are similar to those from Configuration 2. The posterior mean and interval coverage for general Bayesian calibration under the L^2 loss are close to θ_{L^2} and 95%, respectively. There is decreasing bias in the posterior mean for general Bayesian calibration under the OLS loss and traditional Bayesian calibration. This leads to interval under-coverage for the OLS loss. However, the inflated posterior variance under traditional Bayesian calibration leads to over-coverage. This can be seen from the fact that $L_{L^2}(\theta_{L^2}) = 0.1387$, $\sigma^2 = 0.02^2$, leading to $\tau_{SI}^2 = 0.1391$.

Now consider when the support for the design is $\mathcal{X}' = [0, 0.8]$. The posterior mean and interval coverage for general Bayesian calibration under the L^2 loss does converge to θ_{L^2} and 95%, respectively. However, the convergence is slower than for when the design support was $\mathcal{X} = [0, 1]$. As expected, the posterior mean for general Bayesian calibration under the OLS loss and for traditional Bayesian calibration converges to $\theta'_{L^2} = 4.0514$. This bias (between θ_{L^2} and θ'_{L^2}) causes 0% coverage of the intervals, even accounting for the inflated posterior variance under traditional Bayesian calibration.

Configuration 4 The results for Configuration 4 are summarised by Figure 4. The three columns correspond to θ_1 , θ_2 and θ_3 , respectively. The organisation of the figure rows are identical to those for Configurations 1 to 3.

The first conclusion to draw is that there is negligible difference between magnitude and curvature scaling.

The generalised posterior means of $\boldsymbol{\theta}$ converge to the true values θ_{L^2} as n increases. For large n , the mean generalised posterior means for OLS and traditional Bayesian inference become close, as expected from Section 5.2. Also, as expected from Section 5.2, the mean posterior standard deviation of traditional Bayesian inference is larger than under the L^2 and OLS calibration approaches. This leads to over-coverage of the HPD

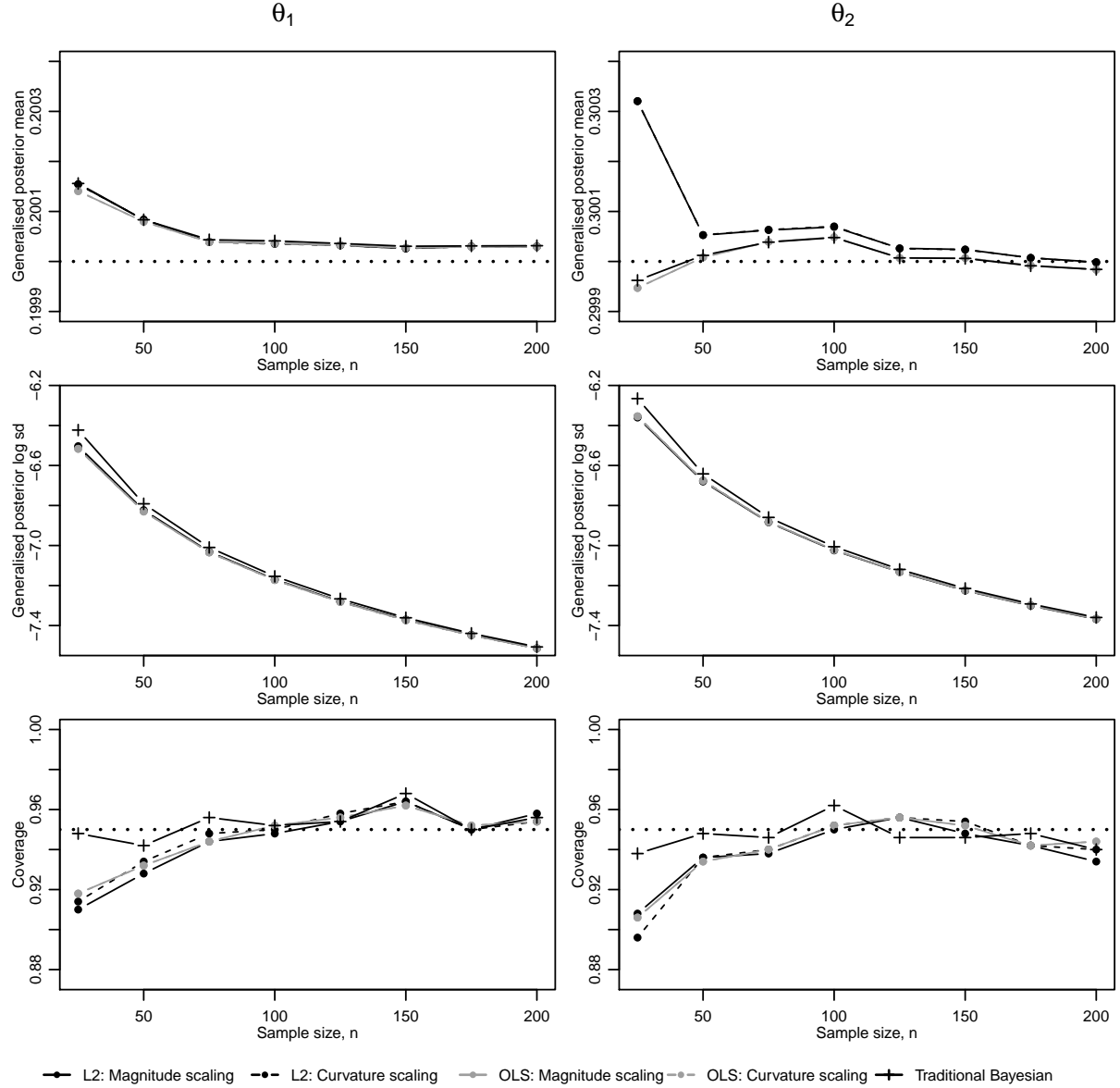


Figure 2: Results for Configuration 1 for θ_1 (left-hand panels) and θ_2 (right-hand panels). The first and second rows show the mean (over the 500 repetitions of the simulation study) generalised posterior mean and log standard deviation, respectively, plotted against n for the five different calibration approaches. The third row shows the coverage of 95% highest generalised posterior density intervals plotted against n .

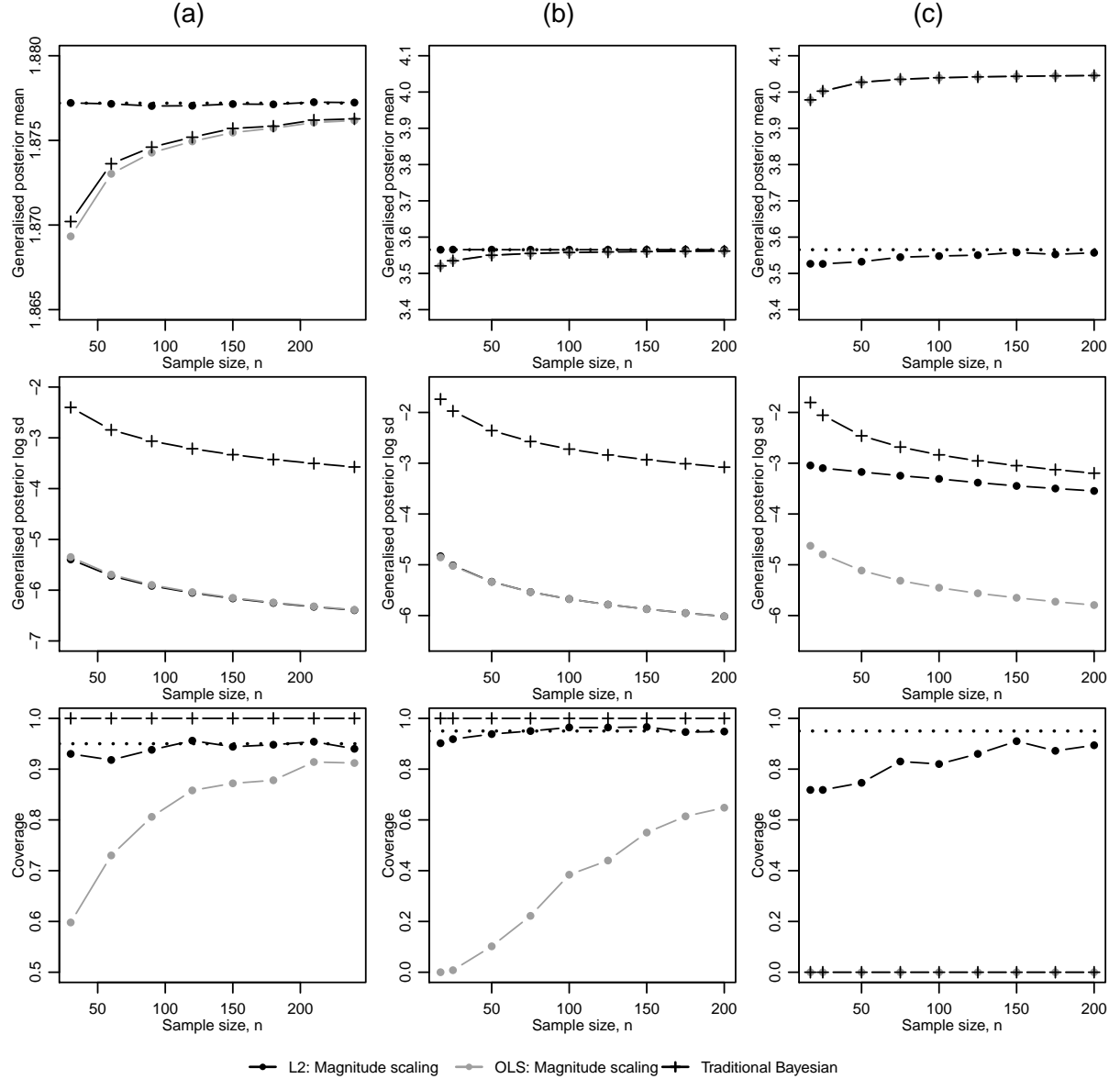


Figure 3: Results for (a) Configuration 2; (b) Configuration 3 with design specification (i) $\mathcal{X} = [0, 1]$; and (c) Configuration 3 with design specification (ii) $\mathcal{X}' = [0, 0.8]$. The first and second rows show the mean (over the 500 repetitions of the simulation study) generalised posterior mean and log standard deviation, respectively, plotted against n for the five different calibration approaches. The third row shows the coverage of 95% highest generalised posterior density intervals plotted against n .

intervals for traditional Bayesian inference. However, the posterior variance inflation is not as significant as in Configurations 2 and 3. This can be seen from the fact that in Configuration 4, $L_{L^2}(\boldsymbol{\theta}_{L^2}) = 0.5222$, $\sigma^2 = 0.7430$, leading to $\tau_{SI}^2 = 1.265$, i.e. $L_{L^2}(\boldsymbol{\theta}_{L^2})$ does not dominate σ^2 as it does in Configurations 2 and 3.

6.1.4 Discussion

From the simulation studies, there was limited difference in terms of long-run performance between curvature and magnitude scaling.

There appeared to be some evidence (from Configurations 2 and 3) to support the use of general Bayesian L^2 calibration over OLS. The mean posterior mean and coverage of HPD intervals are significantly closer to the true value of θ_{L^2} and 95%, respectively, for all but very large n . In Configuration 3, the advantage of the L^2 approach is due to the situation of being unable to select input variables for the experiment from some region of the input space.

Traditional Bayesian inference performs similarly to L^2 and OLS calibration when the mathematical model is true (Configuration 1) but the posterior distribution for the calibration parameters exhibits inflated posterior variance when the mathematical model is not true (Configurations 2 to 4) manifesting itself in over-coverage of the HPD intervals. As predicted from Section 5.1, the degree of inflated posterior variance is controlled by the relative magnitude of σ^2 and $L_{L^2}(\boldsymbol{\theta}_{L^2})$.

In the remainder of this section, We further investigate the different calibration approaches on real applications.

6.2 Ion channels of cardiac cells

The following example comes from Plumlee et al. (2016). The data were collected to learn about ion channels of cardiac cells. The experiment involved measuring the response (the current through sodium channels in the cardiac cell membrane) required to maintain a fixed potential at a given time (the $k = 1$ controllable variable). We consider a subset of the data as considered by Plumlee (2017) and Xie and Xu (2021). This consists of $n = 19$ measurements. Following Plumlee (2017), we set the input x to be the logarithm of time scaled to $\mathcal{X} = [0, 1]$, where the original log-time measurements were on the interval $[-1.75, 3]$.

The mathematical model is

$$\eta(x, \boldsymbol{\theta}) = \mathbf{e}_1^T \text{mexp}[A(x, \boldsymbol{\theta})] \mathbf{e}_4, \quad (24)$$

where $\text{mexp}[\cdot]$ denotes the matrix exponential,

$$A(x, \boldsymbol{\theta}) = \exp(x) \begin{pmatrix} -\theta_2 - \theta_3 & \theta_1 & 0 & 0 \\ \theta_2 & -\theta_1 - \theta_2 & \theta_1 & 0 \\ 0 & \theta_2 & -\theta_1 - \theta_2 & \theta_1 \\ 0 & 0 & \theta_2 & \theta_1 \end{pmatrix},$$

$\boldsymbol{\theta} = (\theta_1, \dots, \theta_3)^T$ (i.e. $p = 3$), and \mathbf{e}_j is the 4×1 vector with j th element equal to one and all other elements zero. The prior distribution for $\boldsymbol{\theta}_{L^2}$ is such that the elements are independent with

$$\theta_{L^2,1} \sim \text{U}[0, 10]; \quad \theta_{L^2,2} \sim \text{U}[0, 10]; \quad \theta_{L^2,3} \sim \text{U}[0, 10].$$

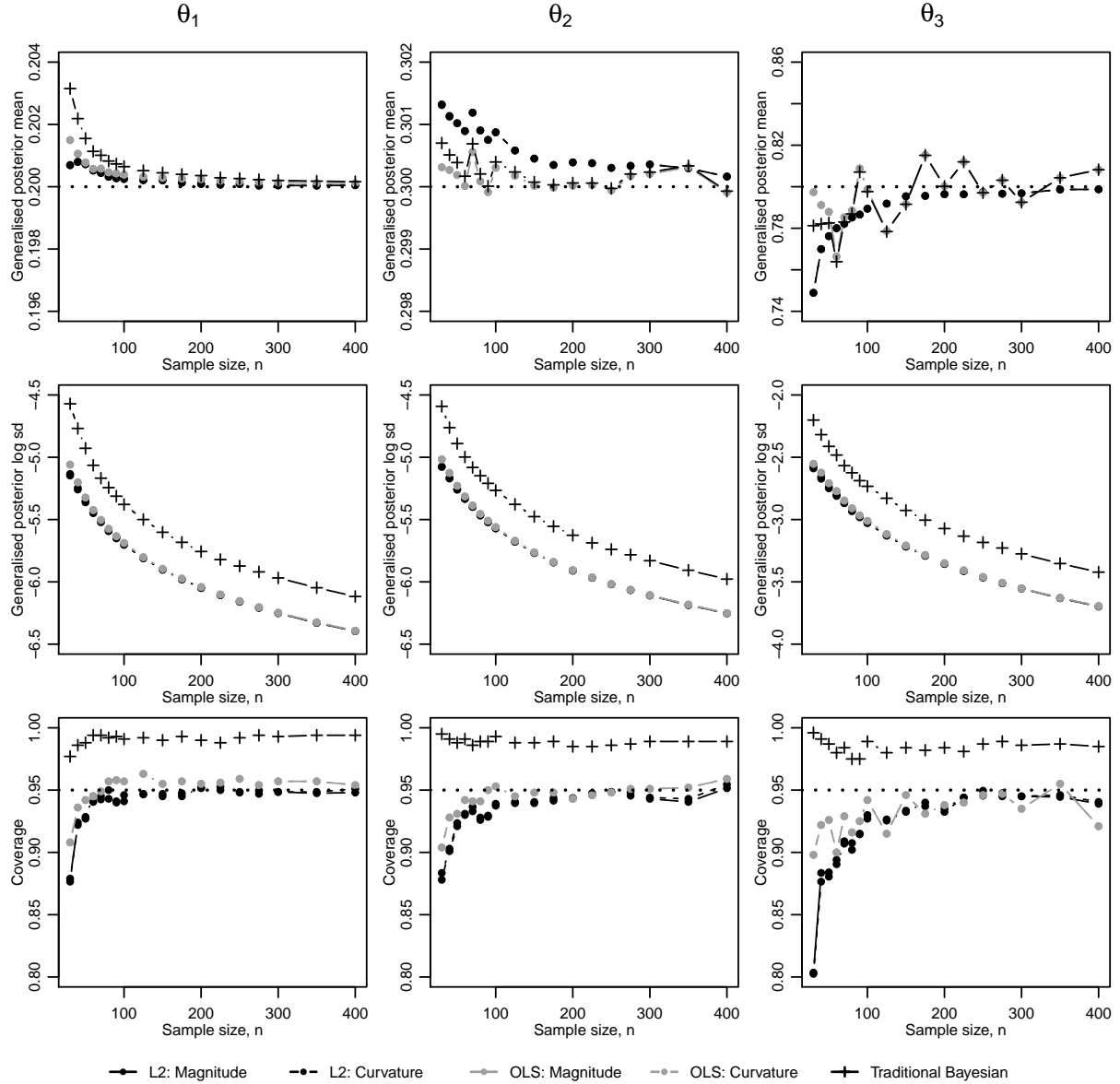


Figure 4: Results for Configuration 4 for θ_1 (left column), θ_2 (centre) and θ_3 (right). The first and second rows show the mean (over the 500 repetitions of the simulation study) generalised posterior mean and log standard deviation of θ plotted against n under L^2 and OLS calibration and under magnitude and curvature scaling. The third row shows the coverage of 95% highest generalised posterior density intervals plotted against n .

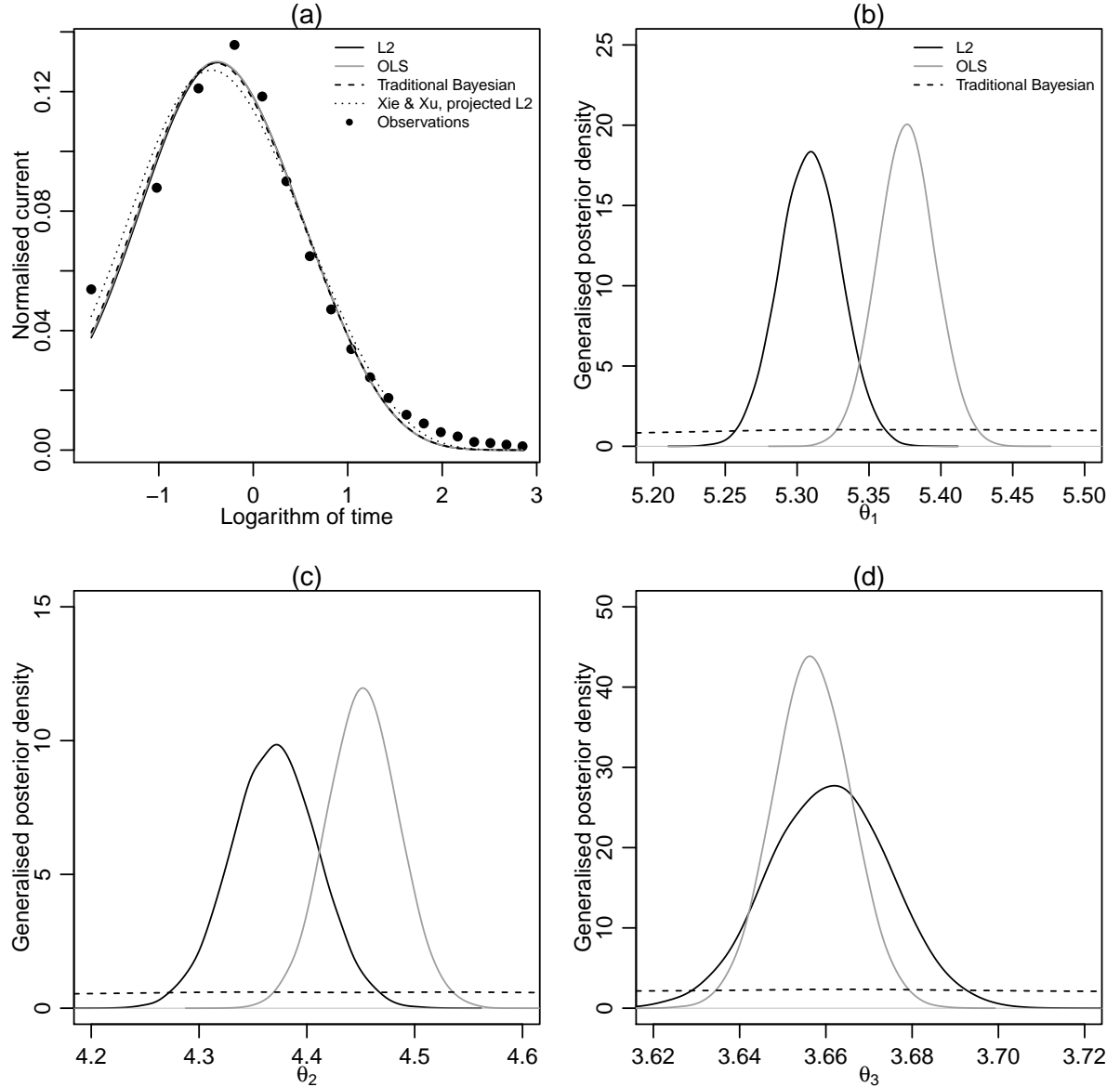


Figure 5: Panel (a) shows a plot of the observed values of the normalised current (y_1, \dots, y_n) against logarithm of time (x_1, \dots, x_n). It also shows the mean of $\eta(\boldsymbol{\theta}_i, x)$ plotted against x for each of L^2 and OLS calibration for both scaling approaches, where $\{\boldsymbol{\theta}\}_{i=1}^M$ denotes the sample from the generalised posterior distribution. Panel (b) shows the generalised posterior densities for θ_1 , θ_2 and θ_3 .

	L^2 magnitude	L^2 curvature	OLS magnitude	OLS curvature	Traditional Bayesian	Xie & Xu projected L^2
θ_1	5.31 (0.0212)	5.31 (0.0290)	5.38 (0.0195)	5.38 (0.0205)	5.47 (0.424)	6.01 (1.20×10^{-5})
θ_2	4.37 (0.0401)	4.37 (0.0485)	4.45 (0.0331)	4.45 (0.0351)	4.60 (0.716)	5.58 (6.00×10^{-6})
θ_3	3.66 (0.0138)	3.66 (0.0102)	3.66 (0.00896)	3.66 (0.00908)	3.66 (0.187)	3.501 (6.00×10^{-6})
OLS ($\times 10^{-5}$)	3.39	3.39	3.38	3.38	3.40	3.98

Table 1: Top: Generalised posterior mean (standard deviation) for θ_1 , θ_2 and θ_3 for the five different calibration methods considered in this paper and Xie and Xu (2021)'s projection approach. Bottom: OLS statistic evaluated at the posterior mean for all methods.

Figure 5(a) shows a plot of the observed values of the normalised current (y_1, \dots, y_n) against logarithm of time. We apply the five different calibration methods listed in Section 6.1.1. In each case, an MCMC sample of size 100,000 is generated from each (generalised) posterior distribution.

Table 1 shows the posterior mean and standard deviation for each of the $p = 3$ calibration parameters for each of the five calibration methods. Also shown are the corresponding statistics taken from Xie and Xu (2021) for the same dataset. Similar to the simulation studies in Section 6.1, there is very small difference between magnitude and curvature scaling.

Figures 5(b)-(d) show the posterior densities for θ_1 , θ_2 and θ_3 , respectively, for general Bayesian calibration under the L^2 and OLS loss functions with magnitude scaling (curvature scaling is omitted for clarity), and traditional Bayesian calibration. There is reasonable agreement between the general Bayesian calibration under L^2 and OLS loss functions with overlap of the posterior densities. The posterior distribution under traditional Bayesian calibration exhibits high variance. Unlike the simulation studies we cannot compare $L_{L^2}(\boldsymbol{\theta}_{L^2})$ and σ^2 . However, we can estimate these values by $\ell_{L^2}(\hat{\boldsymbol{\theta}}_{L^2}) = 3.712 \times 10^{-5}$ and $\hat{\sigma}^2 = 1.029 \times 10^{-7}$, respectively. Hence, we estimate $L_{L^2}(\boldsymbol{\theta}_{L^2})$ to be two orders of magnitude greater than σ^2 , thus explaining the inflated posterior variance.

From the summary statistics in Table 1 from Xie and Xu (2021) shows that their posterior distribution is very different (both in terms of location and scale) to those from the methods developed in this paper. To investigate this we calculate the OLS loss value, $\ell_{OLS}(\boldsymbol{\theta}; \mathbf{y})$, for $\boldsymbol{\theta}$ equal to the posterior mean under the six different methods under consideration. We chose to compare using the OLS loss function since this does not rely on $\hat{\mu}(\cdot)$. The values of the OLS loss are shown in the lower part of Table 1. The methods proposed in this paper result in lower OLS loss value than that in Xie and Xu (2021). However, the difference between the methods on the response scale is quite small. This is evidenced by Figure 5(a) which includes $\eta(x, \boldsymbol{\theta})$ plotted against x where $\boldsymbol{\theta}$ is given by the posterior mean under the different methods.

6.3 Wiffle balls

The following example comes from Gramacy (2020, Section 8.1.2). The experiment measured the time (y in s) for a wiffle ball to freefall a height (in the range $[0.175, 4.275]$ in m, on the original scale). There are 3 replications of each of 21 different heights giving $n = 63$. Figure 6(a) shows a plot of the observed response, y , against height.

The mathematical model is derived incorporating non-linear air resistance (where the force due to air resis-

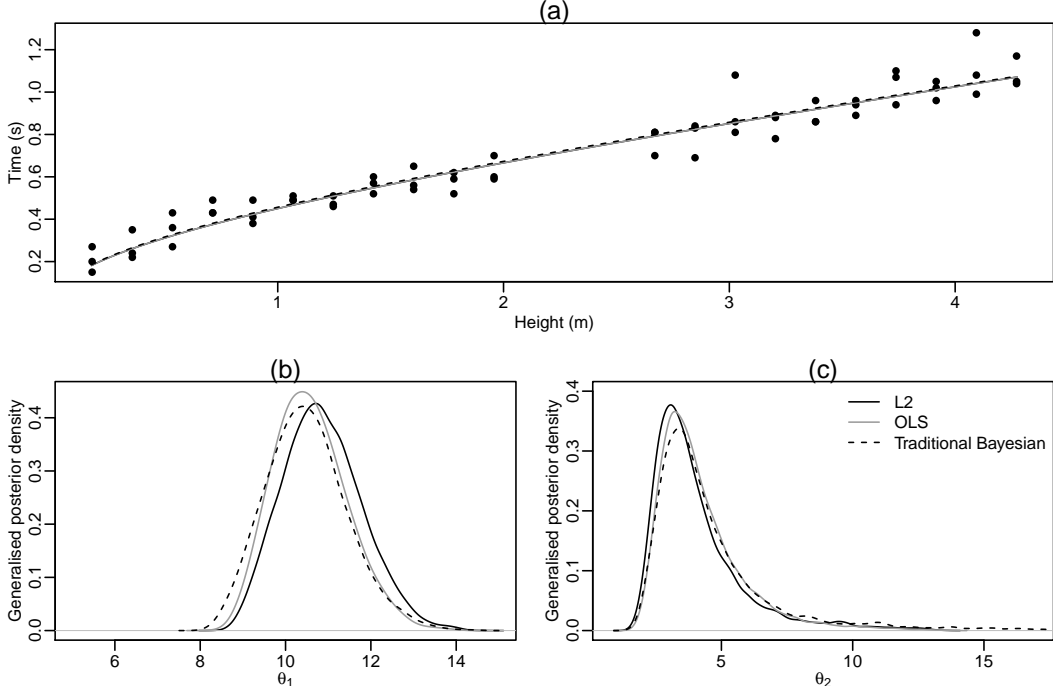


Figure 6: Panel (a) shows a plot of time against height. The lower panels show the generalised posterior densities of θ_1 (b) and θ_2 (c) for general Bayesian calibration under the L^2 and OLS losses with magnitude scaling and traditional Bayesian calibration. Panel (a) also shows a plot of $\eta(x, \theta)$ plotted against x where θ is the posterior mean from these three calibration methods.

	L^2 magnitude	L^2 curvature	OLS magnitude	OLS curvature	Traditional Bayesian
θ_1	10.9 (0.926)	10.9 (0.916)	10.6 (0.860)	10.6 (0.860)	10.5 (0.946)
θ_2	4.06 (1.76)	4.10 (1.77)	4.19 (1.62)	4.19 (1.62)	4.57 (2.35)

Table 2: Generalised posterior mean (standard deviation) for θ_1 and θ_2 for the five different calibration methods.

tance is proportional to the square of the wiffle ball velocity) and is given by

$$\eta(x, \boldsymbol{\theta}) = \sqrt{\frac{\theta_2}{\theta_1}} \operatorname{arccosh} \left[\exp \left(\frac{x_2}{\theta_2} \right) \right].$$

The parameter θ_1 is nominally the acceleration due to gravity and θ_2 is related to the air resistance and mass of the wiffle balls. The prior distribution for $\boldsymbol{\theta}_{L^2}$ is such that the elements are independent with

$$\theta_{L^2,1} \sim U[0, 20]; \quad \theta_{L^2,2} \sim U[0, 20].$$

Figure 6(a) shows a plot of the observed values of time (y_1, \dots, y_n) against height. We apply the five calibration methods listed in Section 6.1.1. In each case, we generate an MCMC sample of size 100,000 from the posterior distribution. Table 2 shows the posterior mean and standard deviation for θ_1 and θ_2 for each of the five methods. Figures 6(b) and (c) show plots of the posterior densities of θ_1 and θ_2 , respectively, for general Bayesian calibration under the L^2 and OLS loss functions with magnitude scaling (curvature scaling is omitted for clarity), and traditional Bayesian calibration.

There is very strong agreement across the different calibration methods. In particular, there is no posterior variance inflation for traditional Bayesian calibration. Consider the estimates of $L_{L^2}(\boldsymbol{\theta}_{L^2})$ and σ^2 given by $\ell_{L^2}(\hat{\boldsymbol{\theta}}_{L^2}; \mathbf{y}) = 4.013 \times 10^{-4}$ and $\hat{\sigma}^2 = 4.726 \times 10^{-3}$, respectively. Since σ^2 is estimated to be an order of magnitude greater than $L_{L^2}(\boldsymbol{\theta}_{L^2})$, it explains the lack of posterior variance inflation.

6.4 Radiative shock hydrodynamics

The application in this example is described in Gramacy (2020, Section 2.2). The data were collected to learn about radiative shocks which arise from astrophysical phenomena.

The physical experiment involves a high energy laser irradiating a beryllium disk at the front of a tube filled with Xenon gas. This causes a high speed shock wave to travel down the tube. The response is the shock location, i.e. the distance travelled down the tube by the shock wave in a predetermined time.

The physical experiment consists of $n = 20$ runs and $k = 4$ inputs are varied: laser energy (in [3750, 3889.6] J), Xenon gas pressure (in [1.032, 1.311] atm), tube diameter (in [0.575, 1.150] mm) and time (in [13, 28] ns). All ranges for input variables are on the original scale. Let x_1, x_2, x_3, x_4 denote the inputs laser energy, Xenon gas pressure, tube diameter and time scaled to [0, 1], respectively.

The mathematical model is given by the predictive mean of a Gaussian process surrogate model fitted to the input and output of a computer experiment. The computer model outputs a theoretical prediction of the shock location based on 10 inputs. The inputs are 2 calibration parameters (electron flux limiter, $\theta_1 \in [0.04, 0.1]$; and energy scale factor, $\theta_2 \in [0.4, 1.1]$), the $k = 4$ controllable variables varied in the physical experiment and a further four variables. The additional four variables are held fixed in the physical experiment but varied in the computer experiment. The prior distribution for $\boldsymbol{\theta}_{L^2}$ is such that the elements are independent with

$$\theta_{L^2,1} \sim U[0.04, 0.1]; \quad \theta_{L^2,2} \sim U[0.4, 1.1].$$

The computer experiment consists of over 26,000 runs. This is too large to feasibly fit a Gaussian process surrogate model. Instead, we create a sub-design of 500 runs. This is accomplished by constructing a maximin Latin hypercube (LH) design of 500 points in the 10 input variables. Then for each point in the LH design, we find the nearest design point (by Euclidean distance) in the computer experiment design. The Gaussian process surrogate model was implemented using the R package `RobustGASP` using a Gaussian correlation function.

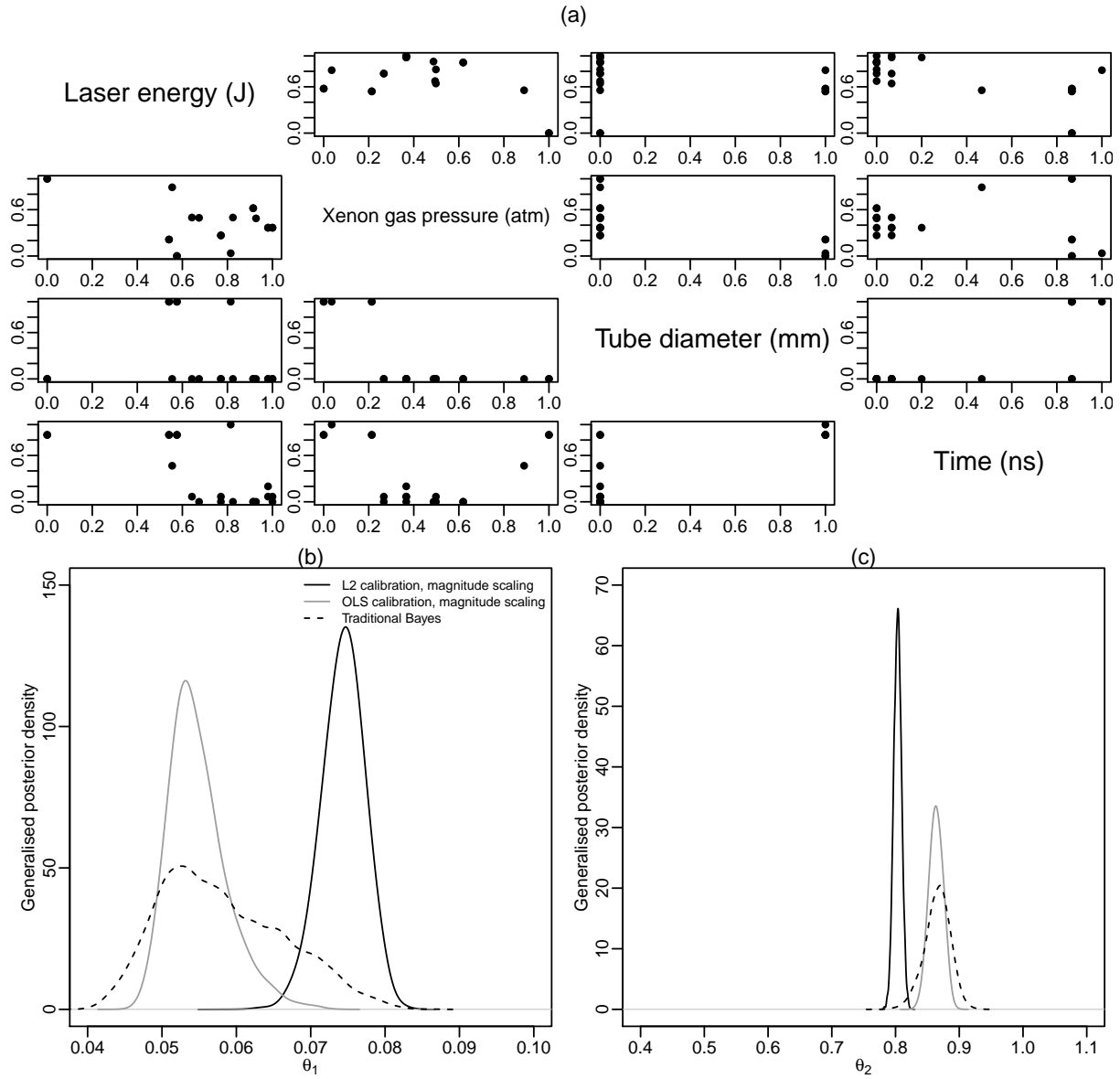


Figure 7: The upper panels show the design points of the physical experiment. The lower panels show the generalised posterior density of θ_1 and θ_2 for L^2 and OLS calibration under magnitude and curvature scaling.

	L^2 magnitude	L^2 curvature	OLS magnitude	OLS curvature	Traditional Bayesian
θ_1	0.0744 (0.00286)	0.0744 (0.00198)	0.0549 (0.00391)	0.0550 (0.00381)	0.0582 (0.00829)
θ_2	0.803 (0.00603)	0.803 (0.00787)	0.864 (0.0105)	0.864 (0.0103)	0.866 (0.0203)

Table 3: Generalised posterior mean (standard deviation) for θ_1 and θ_2 .

Figure 7(a) shows a plot of the design points, $\mathbf{x}_1, \dots, \mathbf{x}_n$, of the physical experiment. The design points do not cover \mathcal{X} as well as could be expected from, for example, a LH design. This impacts the fit of the non-parametric regression model. We found the fit could be improved significantly (based on leave-one-out diagnostics) by including a linear term for scaled time, x_4 , as well as including an intercept. Let $\mathbf{f}(\mathbf{x}) = (1, x_4)^T$ and let F be the $n \times 2$ matrix with i th row given by $\mathbf{f}(\mathbf{x}_i)^T$, for $i = 1, \dots, n$. Furthermore, let $\hat{\boldsymbol{\beta}} = (F^T F)^{-1} F^T \mathbf{y}$ be the ordinary least squares estimators of the parameters associated with the linear model given by $\mathbf{f}(\mathbf{x})^T$, and let $H = F(F^T F)^{-1} F^T$ be the hat matrix.

Now

$$\hat{\mu}(\mathbf{x}) = \mathbf{f}(\mathbf{x})^T \hat{\boldsymbol{\beta}} + \sum_{i=1}^n s_i(\mathbf{x}) \left(y_i - \mathbf{f}(\mathbf{x}_i)^T \hat{\boldsymbol{\beta}} \right),$$

where $\boldsymbol{\rho}$ are estimated as

$$\hat{\boldsymbol{\rho}} = \arg \min \frac{\mathbf{y}^T (I_n - H - S - SH)^2 \mathbf{y}}{[1 - 2/n - \text{tr}(S)/n]^2}.$$

The estimators \hat{W}_{L^2} and $\hat{\sigma}^2$ are adjusted to

$$\begin{aligned} \hat{W}_{L^2} &= 4\hat{\sigma}^2 n \int_{\mathcal{X}} \frac{\partial \eta(\mathbf{x}, \hat{\boldsymbol{\theta}}_{L^2})}{\boldsymbol{\theta}} [\mathbf{s}(\mathbf{x}) + F(F^T F)^{-1} \mathbf{f}(\mathbf{x})]^T d\mathbf{x} \int_{\mathcal{X}} [\mathbf{s}(\mathbf{x}) + F(F^T F)^{-1} \mathbf{f}(\mathbf{x})] \frac{\partial \eta(\mathbf{x}, \hat{\boldsymbol{\theta}}_{L^2})}{\boldsymbol{\theta}^T} d\mathbf{x} \\ \hat{\sigma}^2 &= \frac{\sum_{i=1}^n (y_i - \hat{\mu}(\mathbf{x}_i))^2}{n - 2 - \text{tr}(S)}, \end{aligned} \quad (25)$$

respectively.

Table 3 shows the posterior mean and standard deviation for θ_1 and θ_2 for the five different calibration methods. As the previous examples, there is limited difference between magnitude and curvature scaling for the general Bayesian methods.

Figures 7 (b) and (c) show the posterior densities for θ_1 and θ_2 , respectively, for general Bayesian calibration under the L^2 and OLS loss functions with magnitude scaling (curvature scaling is omitted for clarity), and traditional Bayesian calibration. The scale of the x -axis for Figures 7 (b) and (c) are chosen to match the support for the prior distribution of the elements of $\boldsymbol{\theta}_{L^2}$, respectively.

In terms of location, there is now less agreement between the methods (general Bayesian calibration under the L^2 loss compared to the other methods). We address this issue at the end of this section.

Traditional Bayesian calibration again appears to exhibit posterior variance inflation. Consider the estimates of $L_{L^2}(\boldsymbol{\theta}_{L^2})$ and σ^2 given by $\ell_{L^2}(\hat{\boldsymbol{\theta}}_{L^2}; \mathbf{y}) = 1.650 \times 10^{-3}$ and $\hat{\sigma}^2 = 3.865 \times 10^{-4}$, respectively. Since $L_{L^2}(\boldsymbol{\theta}_{L^2})$ is estimated to be an order of magnitude greater than σ^2 , it explains the posterior variance inflation.

The results from general Bayesian calibration under the L^2 loss should be viewed sceptically due to the construction of $\hat{\mu}(\mathbf{x})$ with the inclusion of linear terms. Indeed, the scale of the posterior for the general Bayesian calibration under the OLS loss is questionable due to its dependence on $\hat{\sigma}^2$. However, of the $n = 20$ design points there are actually 16 unique design points. This allows a model-independent estimate of σ^2 (see, for example, Gilmour and Trinca 2012) to be calculated as $\hat{\sigma}^2 = 4.003 \times 10^{-4}$, i.e. close to that found using (25).

7 Discussion

This paper proposes generalised Bayesian approaches for the calibration of mathematical models, namely L^2 and OLS calibration. In each case, two methods are developed to scale the generalised posterior distribution

to maintain frequentist properties. The proposed approaches were validated using simulation studies in Section 6.1 before being applied to real problems in Sections 6.2 to 6.4.

Compared to competing Bayesian L^2 calibration approaches, the advantages of the proposed methodology are as follows.

- Compared to Xie and Xu (2021), a known distribution is not required to be specified for y_1, \dots, y_n (or equivalently e_1, \dots, e_n).
- Compared to Plumlee (2017), we do not need to constrain the Gaussian process prior distribution for the bias function, $\delta(\mathbf{x})$.
- Compared to Woody et al. (2019), there is no computationally expensive bootstrapping to perform to determine γ for the magnitude scaling.

There are several topics for further investigation. An issue that needs addressing is the design of the physical experiment. In the Radiative shock hydrodynamics application in Section 6.4, the design of the physical experiment necessitating the use of a linear term in the non-parametric smoother. Future work will consider the design of the physical experiment for generalised Bayesian calibration of mathematical models. One possible approach could be an extension of the Bayesian decision-theoretic approach (see, for example, Chaloner and Verdinelli 1995) to design of experiments for general Bayesian calibration. One hurdle will be that the Bayesian decision-theoretic approach relies on a full probability model which is notably absent for general Bayesian inference.

The automatic scaling methods rely on a point estimate of σ^2 . An extension of the methodology would be to consider quantifying the uncertainty in this estimation. For example, let $\pi_M^S(\boldsymbol{\theta}|\mathbf{y}, \sigma^2)$ denote the generalised posterior under loss M and scaling S , conditional on a fixed value of σ^2 . Then let $\pi(\sigma^2|\mathbf{y}, \sigma^2)$ denote the posterior distribution of σ^2 found via, for example, assuming a Gaussian process smoother for $\mu(\mathbf{x})$ as done by Xie and Xu (2021). Then the marginal generalised posterior distribution for the calibration parameters could be obtained via

$$\pi_M^S(\boldsymbol{\theta}|\mathbf{y}) = \int_0^\infty \pi_M^S(\boldsymbol{\theta}|\mathbf{y}, \sigma^2) \pi(\sigma^2|\mathbf{y}) d\sigma^2.$$

For general Bayesian L^2 calibration under the L^2 loss, a computational approach that combines the approximation of the integral in the L^2 loss and the MCMC method could be considered. A potential such approach is a pseudo-marginal Metropolis-Hastings algorithm (see, for example, Andrieu and Roberts 2009). This is where evaluation of the analytically intractable generalised likelihood

$$\pi_{L^2}^S = \exp[-n\ell_{L^2}^S(\boldsymbol{\theta}; \mathbf{y})]. \quad (26)$$

is replaced in the acceptance probability by an unbiased estimate. In this case the algorithm targets the true posterior distribution of the calibration parameters. However, although an unbiased estimate for $\ell_{L^2}^S(\boldsymbol{\theta}; \mathbf{y})$ is trivial to produce, the same is not true for the generalised likelihood (26). One possible approach could be to use a Russian Roulette debiasing scheme (see, for example, Lyne et al. 2015).

References

Andrieu, C. and Roberts, G. (2009) The pseudo-marginal approach for efficient monte carlo computations. *Annals of Statistics* **37**, 697–725.

Ba, S. and Joseph, V. R. (2018) *MaxPro: Maximum Projection Designs*. URL <https://CRAN.R-project.org/package=MaxPro>. R package version 4.1-2.

Billingsley, P. (1995) *Probability and Measure*. New York: John Wiley and Sons 3 edn.

Bissiri, P., Holmes, C. and Walker, S. (2016) A general framework for updating belief distributions. *Journal of the Royal Statistical Society Series B* **78**, 1103–1130.

Chaloner, K. and Verdinelli, K. (1995) Bayesian experimental design: a review. *Statistical Science* **10**, 273–304.

Georgiev, A. A. (1988) Consistent nonparametric multiple regression: The fixed design case. *Journal of Multivariate Analysis* **25**, 100–110.

Gilmour, S. and Trinca, L. (2012) Optimum design of experiments for statistical inference (with discussion). *Journal of the Royal Statistical Society Series C* **61**, 345–401.

Gramacy, R. B. (2020) *Surrogates: Gaussian Process Modeling, Design and Optimization for the Applied Sciences*. Boca Raton, Florida: Chapman Hall/CRC.

Gu, M. and Wang, L. (2018) Scaled Gaussian stochastic process for computer model calibration and prediction. *SIAM/ASA Journal of Uncertainty Quantification* **6**, 1555–1583.

Joseph, V., Gul, E. and Ba, S. (2015) Maximum projection designs for computer experiments. *Biometrika* **102**, 371–380.

Kennedy, M. and O'Hagan, A. (2001) Bayesian calibration of computer models (with discussion). *Journal of the Royal Statistical Society Series B* **63**, 425–464.

Lange, K. (2010) *Numerical Analysis for Statisticians*. Springer-Verlag, New York 2nd edn.

Lyne, A.-M., Girolami, M., Y., A., Strathmann, H. and Simpson, D. (2015) On Russian roulette estimates for Bayesian inference with doubly-intractable likelihoods. *Statistical Science* **30**, 443–467.

Miller, J. (2021) Asymptotic normality, concentration, and coverage of generalized posteriors. *Journal of Machine Learning Research* **22**, 1–53.

O'Hagan, A. and Forster, J. (2004) *Kendall's Advanced Theory of Statistics Volume 2B Bayesian Inference*. Wiley 2nd edn.

Pauli, F., Racugno, W. and Ventura, L. (2011) Bayesian composite marginal likelihoods. *Statistica Sinica* **21**, 149–164.

Plumlee, M. (2017) Bayesian calibration of inexact computer models. *Journal of the American Statistical Association* **112**, 1274–1285.

Plumlee, M., Joseph, V. and Yang, H. (2016) Calibrating functional parameters in the ion channel models of cardiac cells. *Journal of the American Statistical Association* **111**, 500–509.

Ribatet, M., Cooley, D. and Davison, A. (2012) Bayesian inference from composite likelihoods with an application to spatial extremes. *Statistica Sinica* **22**, 813–845.

Roberts, G. and Rosenthal, J. (2001) Optimal scaling of various metropolis-hastings algorithms. *Statistical Science* **16**, 351–367.

Tuo, R. and Wu, C. (2015) Efficient calibration for imperfect computer models. *Annals of Statistics* **43**, 2331–2352.

— (2016) A theoretical framework for calibration in computer models: Parametrization, estimation and convergence properties. *SIAM/ASA Journal of Uncertainty Quantification* **4**, 767–795.

Wahba, G. (1990) *Spline models for observational data* vol. 59. Society for Industrial Mathematics.

Wilkes, S. (1932) Certain generalizations in the analysis of variance. *Biometrika* **24**, 471–494.

Wong, R., Storlie, C. and Lee, T. (2017) A frequentist approach to computer model calibration. *Journal of the Royal Statistical Society Series B* **79**, 635–648.

Woody, S., Ghaffari, N. and Hund, L. (2019) Bayesian model calibration for extrapolative prediction via Gibbs posteriors. *arXiv:1909.05428v1*.

Xie, F. and Xu, Y. (2021) Bayesian projected calibration of computer models. *Journal of the American Statistical Association* **536**, 1965–1982.